https://doi.org/10.5194/egusphere-2026-7134
Preprint. Discussion started: 26 November 2026
© Author(s) 2026. CC BY 4.0 License.

Glacier changes across Subantarctic Heard Island revealed by remote sensing and ice thickness inversions

Weilin Yang[1,2], Levan G. Tielidze[1,2,3], Regine Hock[4,5], Bethan J. Davies[6], Steven L. Chown[7], Duane D. McKenna[8], Sarah S. Thompson[9], Justine D. Shaw[10], Andrew N. Mackintosh[1,2]

[1]School of Earth, Atmosphere and Environment, Faculty of Science, Monash University, Clayton, Melbourne, VIC 3800, Australia
[2]Securing Antarctica's Environmental Future, School of Earth, Atmosphere and Environment, Monash University, Clayton, Melbourne, VIC 3800, Australia
[3]Glaciology Research Centre, School of Natural Sciences and Medicine, Ilia State University, Tbilisi 0179, Georgia
[4]Department of Geosciences, University of Oslo, Oslo 0316, Norway
[5]Geophysical Institute, University of Alaska, Fairbanks, Fairbanks, Alaska 99775-7320, USA
[6]School of Geography, Politics and Sociology, Newcastle University, Newcastle upon Tyne NE1 7RU, UK
[7]Securing Antarctica's Environmental Future, School of Biological Sciences, Monash University, Victoria, 3800, Australia
[8]Department of Biological Sciences, and Center for Biodiversity Research, University of Memphis, Memphis, TN 38152, USA
[9]Australian Antarctic Program Partnership, Institute for Marine and Antarctic Studies, University of Tasmania, Hobart, TAS 7001, Australia
[10]Securing Antarctica's Environmental Future, Australian Antarctic Division, Department of Climate Change, Energy, the Environment and Water, Kingston 7050, Tasmania, Australia

Correspondence to: Weilin Yang (weilinyang.yang@monash.edu and ywlcwc@gmail.com)

Abstract. Glacier recession is rapidly reshaping glacierized landscapes and the terrestrial, freshwater, and coastal environments they support. However, on remote subantarctic islands such as Heard Island, the magnitude, spatial variability, and control of long-term glacier change remain poorly constrained by the limited observations and outdated glacier inventories used in global products. This study provides an updated, spatially and temporally consistent assessment of glacier area, volume and mass change, and ice thickness, across Heard Island. Our results show that the rates of glacier area and mass loss accelerated by 1.8 times during 2000–2019 compared with 1947–2000, coincident with regional warming. Particularly large changes occurred at lagoon-terminating glaciers such as Stephenson Glacier, illustrating how local terminus geometry and expanding proglacial lagoons can strongly modulate the expression of broader climatic forcing. Sensitivity experiments indicate temporal mismatches between glacier outlines and digital elevation models can bias glacier mass-balance and ice thickness estimates, especially for rapidly receding glaciers. These results highlight the importance of temporally consistent glacier datasets and provide a physical baseline for understanding future landscape and ecological change across Heard Island.

1 Introduction

Glaciers outside the ice sheets are receding and losing mass in response to ongoing global warming, contributing to sea-level rise, altering downstream hydrology, and increasing mountain hazards (Hock et al., 2019; Fox-Kemper et al., 2021). Glacier recession is also greatly reshaping glacierized landscapes and the terrestrial, freshwater, and marine ecosystems they support (Cauvy-Fraunié and Dangles, 2019; Bosson et al., 2023; Davies et al., 2026). Newly exposed land, proglacial lakes, and coastal or marine areas provide new habitats for ecological colonization and ecosystem development (Lee et al., 2017, 2022), while the loss of glacier influence may threaten specialized glacier-dependent species and communities (Cauvy-Fraunié and Dangles, 2019).

Heard Island, part of the World Heritage-listed Heard Island and McDonald Islands in the Southern Indian Ocean (Fig. 1a), is one of the most pristine places on the planet, with minimal human disturbance and important habitats for wildlife (UNESCO, 1997). Despite its extreme remoteness, Heard Island has experienced substantial environmental changes under recent global

https://doi.org/10.5194/egusphere-2026-7134
Preprint. Discussion started: 26 November 2026
© Author(s) 2026. CC BY 4.0 License.

warming (Allison and Keage, 1986; Kiernan and McConnell, 2002; Green and Woehler, 2006; Budd, 2007; Thost and Truffer, 2008; Donoghue, 2009; Tielidze et al., 2025). Glaciers on Heard Island are shrinking rapidly, losing almost a quarter of their size over the past 72 years (Tielidze et al., 2025). The recession was strongly spatially heterogeneous, with glaciers in the eastern sector showing the greater and faster losses. These changes have substantially reorganized the island landscape, with consequences for the evolution of its biotas, the form of its ecosystems, and their interaction, which extend beyond the loss of glacial ice.

Due to the low frequency of research visitation on the island (e.g., Australian Antarctic Programme visits in 1963, 1971, 2000-2001, 2003-2004, and 2025-2026), the characteristics of glacier change on Heard Island, its spatial variability, and the potential controls on these changes remain poorly understood. Information on glacier mass balance and ice thickness for Heard Island has mainly been derived from global-scale datasets, including mass-balance estimates based on digital elevation model (DEM) differencing (Hugonnet et al., 2021), annual mass-balance estimates combining geodetic and glaciological observations (Dussaillant et al., 2025; The WGMS Network, 2026; WGMS, 2026), and inverted ice thickness products (Farinotti et al., 2019; Millan et al., 2022; Maffezzoli et al., 2026; Frank et al., 2026). All these products rely on glacier outlines from the Randolph Glacier Inventory (RGI) v6.0 and v7.0 (RGI Consortium, 2017, 2023). For Heard Island, both RGI versions are based on glacier outlines derived from 1988 medium-resolution (10 and 20 m) SPOT imagery and contain inaccurate terminus positions and ice divides, particularly for glaciers in the eastern sector (Tielidze et al., 2025). Thus, existing estimates of glacier mass balance and ice thickness are not consistent with the updated Heard Island glacier inventory, limiting robust island-wide assessments of glacier change and the reliable initialisation of numerical glacier models.

To address these limitations, we provide a spatially and temporally consistent assessment of glacier change across Heard Island using remote sensing and ice thickness inversion. First, we supplement the inventories of Tielidze et al. (2025) by mapping more outlines of selected eastern glaciers for 2001, 2005 and 2010. Based on these glacier boundaries, NASADEM (NASA JPL, 2020) and Pléiades DEMs (Berthier et al., 2024), mean glacier mass balances from 2000–2019 are recalculated. Ice thicknesses and glacier volumes for 1947, 1988, 2001, and 2019 are calculated from glacier surface slope and basal shear stress based on the perfect-plasticity approximation, enabling us to quantify the mass changes further back to the mid-20th century and account for below-water-level changes. Together, these datasets are used to examine the glacier change across Heard Island and its potential drivers. This work provides not only improved estimates of glacier changes, but also a spatial framework for understanding how the island's terrestrial landscape, and associated ecosystems, is being reorganized through time.

2 Study area

Heard Island (53°05′S, 73°31′E) is a volcanic sub-Antarctic island, dominated by two major volcanoes, the active Big Ben (Mawson Peak at 2745 m above sea level; a.s.l.) and the apparently inactive Mt. Dixon (706 m a.s.l.) on the Laurens Peninsula (Fig. 1). The island is approximately 40 km long, extending from the northwestern tip of the Laurens Peninsula to Spit Bay in the southeast, and about 20 km wide from the north to the south coast, with a reference island area of approximately 368 km^2 (Geoscience Australia, 2026). However, the actual island area may vary over time due to variations in tidewater glacier and coastal lagoon extents, as well as coastal erosion.

Heard Island is heavily glacierized, with 35 individual glaciers covering approximately 61 % of its reference land area in 2019 (Tielidze et al., 2025). Glaciers flow from the Mawson and Anzac peaks, forming two ice complexes. Most of the island's glaciers are concentrated within the larger ice complex on Big Ben, with 22 individual glaciers. During the Last Glacial Maximum (LGM), glaciers may have expanded over the adjacent continental shelf (Hall, 2004; Balco, 2007), and during the earliest documented human visits to the island in the 19th century, glaciers were more extensive than today, with many observers to be marine terminating (Green and Woehler, 2006). Subsequent glacier recession, particularly along the southeastern flank of the island in the 20th and early 21st centuries, led to the development of four major proglacial lagoons:

https://doi.org/10.5194/egusphere-2026-7134
Preprint. Discussion started: 26 November 2026
© Author(s) 2026. CC BY 4.0 License.

Winston, Stephenson, Brown, and Compton (Allison and Keage, 1986; Kiernan and McConnell, 2002; Budd, 2007; Tielidze et al., 2025). In 2019, Heard Island included 8 marine-terminating, 4 lagoon-terminating, and 23 land-terminating glaciers, accounting for 61.6 %, 15.5 %, and 22.9 % of the total glacier area, respectively (Tielidze et al., 2025).

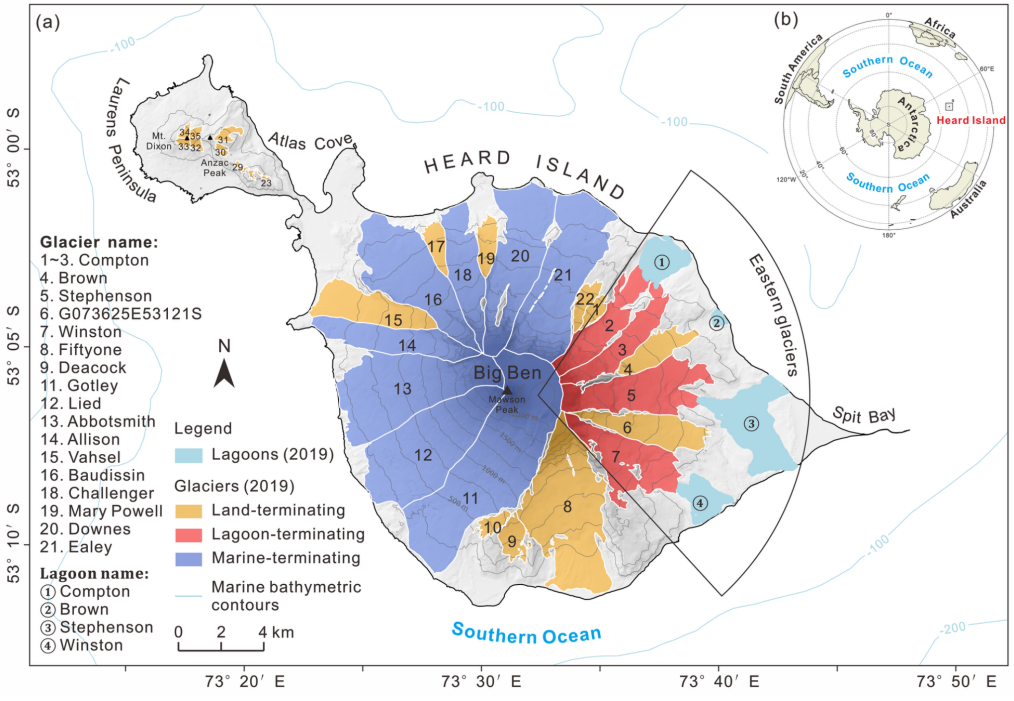

Figure 1. (a) An overview of Heard Island and its glaciers. The 20 m 2018-2019 Pléiades DEMs (Berthier et al., 2024) are used as the background topography, with elevation contours shown as 250 m intervals. The glacier outlines in 2019 are obtained from Tielidze et al. (2025). Eastern glaciers include glaciers Nos. 1–7 based on Tielidze et al. (2025). The marine bathymetric contours were obtained from Harris (2004). **(b)** Location of Heard Island in the Southern Hemisphere.

Heard Island has a relatively well-developed terrestrial fauna, despite significant glacial coverage following the end of the LGM. The largely undisturbed breeding habitats form an important component of the World Heritage and conservation values of the Heard Island and McDonald Islands region (UNESCO, 1997). It is characterised not only by above- and below-ground breeding seabirds, but also by at least 75 plant species, including grasses, cushion plants, a megaherb and bryophytes, and more than 131 invertebrate species (Green and Woehler, 2006). The latter include an insect fauna with unusual constituents, such as marine, and lichen- and moss-feeding weevils (Chown and Klok, 2001).

The plant species are organised into ~seven recognisable communities with pronounced differences between lowland closed vegetation communities and higher elevation open fellfield (Green and Woehler, 2006). Invertebrate communities largely follow these patterns (Chown and Klok, 2001; Davies et al., 2011; Chown et al., 2022). Coastal proximity, elevation, and water availability all play significant roles in structuring communities (Chown and Klok 2003; Chown et al., 2004; Green and Woehler, 2006). While extensive investigations of landscape-related population genomic variation have not been made, it is clear that differences in species composition exist between the eastern and western sides of the island (Green and Woehler, 2006), and it is expected that these would be reprised among areas long-isolated by major glaciers (Baird et al., 2021).

The climate on Heard Island is strongly influenced by variations in the position and strength of the Southern Hemisphere westerlies and associated ocean changes (Thost and Truffer, 2008; Tielidze et al., 2025). The island experiences small seasonal and diurnal temperature variations, persistent cloud cover, frequent precipitation, strong winds, and year-round snowfall. Based on the limited available observations, mean temperature was 1.9 °C at Atlas Cove during 1999–2011 and 2.4 °C at Spit Bay during 1998–2014 (Menne et al., 2012). Mean annual precipitation at Atlas Cove was approximately 1.4 m during 1948–1954,

https://doi.org/10.5194/egusphere-2026-7134
Preprint. Discussion started: 26 November 2026
© Author(s) 2026. CC BY 4.0 License.

whereas nearly 2.0 m was recorded at Spit Bay during 1992–1993 (Green and Woehler, 2006). Orographic effects exert a strong control on the spatial distribution of temperature and precipitation across the island. However, the scarcity of meteorological observations means that these spatial gradients and their temporal variability remain poorly constrained.

3 Data and Methods

This study integrates multi-temporal glacier outlines, satellite imagery, DEMs, and glacier modelling to quantify glacier area, volume and mass changes, and invert ice thickness across Heard Island. The overall workflow is shown in Fig. 2, and the main datasets are summarized in Table 1. All spatial datasets are transformed to a common WGS 84 / UTM zone 43S reference system and resampled to the 20 m Pléiades reference grid when required. This common spatial framework allows glacier area change, mass-balance, ice thickness and volume estimates to be evaluated consistently across the island. In addition, all currently available global-scale products for Heard Island (Hugonnet et al., 2021; WGMS, 2026; Farinotti et al., 2019; Millan et al., 2022; Frank et al., 2026; Maffezzoli et al., 2026) are used for external comparison.

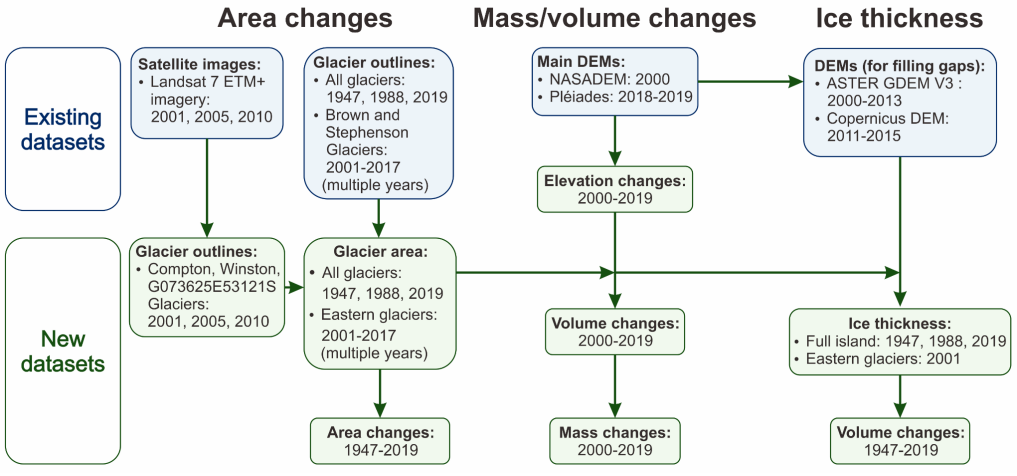

Figure 2. Overview of the existing datasets (see Table 1), and newly generated datasets in this study.

Table 1. Summary of the existing datasets used in this study.

Data	Period/coverage	Native resolution or form	Use in this study	Source
Glacier outlines	All glaciers: 1947, 1988, 2019; Brown and Stephenson: 1947, 1988, 2001, 2003, 2004, 2005, 2008, 2009, 2010, 2017, 2019; Newly mapped eastern glaciers: 2001, 2005, 2010	1947: 1:50,000; Others: 0.5-30 m	Glacier area change assessment; Boundary constraints for mass-balance and ice thickness calculations	Tielidze et al. (2025)
Landsat 7 ETM+ imagery	2001, 2005, 2010	Panchromatic band: 15 m; Six reflective multispectral bands: 30 m	Mapping eastern glaciers	EROS Center (2020)
Pleiades DEMs	2018-2019	0.5-2 m / 20 m	Calculating elevation differences; estimating 2019 ice thickness; definition of the common analysis grid	Berthier et al. (2024)
NASADEM SRTM-only Height and Height Precision Mosaic	11–22 February 2000	1 arc-second spacing (approximately 30 m)	Calculating elevation differences; estimating 1947, 1988 and 2001 ice thickness;	NASA JPL (2020)
Copernicus DEM GLO-30	Mainly 2011-2015 source data	30 m	Fill gaps in the Pleiades 2019 DEM for calculating ice thickness	European Space Agency (2021)
ASTER GDEM V3	Multi-temporal composite derived from ASTER observations acquired between March 2000 and November 2013	1 arc-second spacing (approximately 30 m)	Fill gaps in the NASADEM for calculating ice thickness	NASA/METI/AIST/Japan Space systems and U.S./Japan ASTER Science Team. (2019)
RGI v6.0 and v7.0	1988	Not applicable	Comparison only	RGI Consortium, 2017 and 2023
External mass balance products	2000-2020	Not applicable	Comparison only	Hugonnet et al., 2021; WGMS, 2026
External ice-thickness products	1988	25-100 m	Comparison only	Farinotti et al. (2019); Millan et al. (2022); Frank et al. (2026); Maffezzoli et al. (2026)

https://doi.org/10.5194/egusphere-2026-7134
Preprint. Discussion started: 26 November 2026
© Author(s) 2026. CC BY 4.0 License.

3.1 Glacier outlines

Glacier outlines from Tielidze et al. (2025) provide the main spatial framework for this study, including island-wide glacier inventories for 1947, 1988, and 2019 and more frequent outlines for Brown (No. 4) and Stephenson (No. 5) glaciers (Fig. 1) between 2001 and 2017 (Table 1). However, comparable multi-temporal outlines are not available for the other rapidly receding eastern glaciers. Thus, we mapped Compton (Nos. 1–3), G073625E53121S (No. 6), and Winston (No. 7) glaciers (Fig. 1) for 2001, 2005, and 2010. The satellite images used to map these glaciers were the same as those used by Tielidze et al. (2025), including 15 m resolution panchromatic band of the Landsat 7 Enhanced Thematic Mapper Plus (ETM+) images acquired in 2001, 2005 and 2010 (Table 1; U.S. Geological Survey, 1998). Based on the glacier outlines from Tielidze et al. (2025) and the newly mapped outlines, glacier areas and area changes were quantified.

The boundaries of eastern glaciers were manually delineated following the approach of Tielidze et al. (2025). The 1988 and 2019 glacier outlines from Tielidze et al. (2025) were used as an initial reference and were manually edited against each satellite image. Glacier terminus was identified from the contrast between glacier ice, exposed terrain, lagoon and ocean. Lateral glacier margins were mapped using changes in surface colour, texture, slope, and shadow. Ice divides were kept consistent with the 2019 glacier inventory unless the satellite imagery provided clear evidence of a change in glacier connectivity.

Mapping uncertainty was estimated using the buffer method in Tielidze et al. (2025). This method applies inward and outward buffers to each mapped boundary to define the minimum and maximum plausible glacier areas, from which the area uncertainty is calculated. A 30 m buffer was applied to the 1947 glacier outlines, a 20 m buffer to the 1988 glacier outlines, a 15 m buffer was used for 2001–2010 glacier outlines, and a 10 m buffer to the 2017 and 2019 glacier outlines.

3.2 Glacier mass balance

We calculated glacier mass balance from the elevation differences between NASADEM (NASA JPL, 2020; Fig. S1a) and four Pléiades DEMs (Berthier et al., 2024; Fig. S1b), using the 1988-2019 glacier boundaries as spatial constraints. NASADEM was acquired during the Space Shuttle Endeavour STS-99 mission between 11 and 22 February 2000 at approximately 30 m spatial resolution. We used 16 February 2000, the midpoint of the acquisition period, as the representative date of NASADEM in this study. The Pléiades DEMs were acquired on 22 April 2018, 7 April 2019 (two acquisitions), and 21 November 2019 at 20 m resolution. The four Pléiades DEMs were combined into a single mosaic. Where acquisitions overlapped, the elevation from the newer DEM was retained. All DEMs were projected to WGS 84 / UTM zone 43S and resampled to a 20 m grid.

The NASADEM was co-registered to the Pléiades DEM mosaic using the Nuth–Kääb method implemented in xDEM v0.2.3 (Nuth and Kääb, 2011; xDEM contributors, 2026). For the initial Nuth–Kääb adjustment, stable terrain was defined as land within the Heard Island boundary but outside the 1988 glacier outlines. Here, the land with slopes $< 3°$ and $> 45°$ were excluded from initial Nuth–Kääb adjustment. The initial transformation shifted NASADEM by 22.2 m westward, 14.5 m northward, and −1.6 m vertically. Residual median vertical offsets were estimated over valid stable terrain and removed separately for each of the four Pléiades acquisitions.

A curvature-dependent elevation bias was corrected using maximum curvature derived from the co-registered NASADEM, following Gardelle et al. (2012). Elevation differences over stable terrain were summarized by their median values within 30 equal-width maximum-curvature bins. A polynomial relationship was fitted to the binned elevation differences using xDEM. The resulting relationship was then applied to correct the co-registered NASADEM elevations. Finally, a vertical correction of −1.1 m was applied to NASADEM to remove the remaining median residual over stable terrain. After that, the elevation differences over stable terrain had a median of 0.0 m and a normalized median absolute deviation (NMAD) of 2.9 m.

Based on the co-registered DEMs, we then calculated the glacier surface elevation-change rate (dh/dt; m yr^{-1}). For each pixel containing valid elevations in both DEMs (Fig. S1c), dh/dt was calculated as:

https://doi.org/10.5194/egusphere-2026-7134
Preprint. Discussion started: 26 November 2026
© Author(s) 2026. CC BY 4.0 License.

$$\left(\frac{dh}{dt}\right)_i = \frac{h_{Pléiades,i} - h_{NASADEM,i}}{\Delta t_i}, \quad (1)$$

where Δt_i is the interval between 16 February 2000 and the acquisition date of the Pléiades DEM contributing to pixel *i*. Outliers and missing values in the *dh/dt* were processed using an elevation-band approach, following a hypsometric approach of Hugonnet et al. (2021). For eastern glaciers, the 2001 glacier outlines were divided into 100 m elevation bands using the co-registered NASADEM, whereas the 1988 outlines were used to define the corresponding elevation bands for the western glaciers. Within each elevation band, outliers in the *dh/dt* were identified relative to the band median and excluded when their absolute deviations exceeded five NMAD. The band mean *dh/dt* was calculated from the remaining valid pixels and used to replace outliers and fill missing values within each elevation band. For elevation bands containing no valid *dh/dt* pixels, the band mean was linearly interpolated from adjacent measured bands. At the upper or lower elevations, where interpolation from both sides was not possible, the value from the nearest valid elevation band was assigned.

Glacier volume change rate (*dV/dt*; $m^3\ yr^{-1}$) was calculated from the *dh/dt* values of all pixels within each glacier outline:

$$\frac{dV}{dt} = \sum_{i=1}^{n} \left(\frac{dh}{dt}\right)_i A_{pixel}, \quad (2)$$

where *n* is the total number of 20 m grid cells within each glacier outline, and A_{pixel} is the area of each grid cell (400 m^2). For eastern glaciers, all available glacier outlines between 2001 and 2019 were used independently to extract *dh/dt* and calculate *dV/dt*. We assumed that *dV/dt* varied linearly between consecutive inventory years. For each interval, *dV/dt* was the mean of the *dV/dt* derived from the two bounding glacier outlines, with the duration as the time between their inventory years. The final glacierwide *dV/dt* was calculated as the duration-weighted mean. For western glaciers, where only the 1988 and 2019 outlines were available, *dV/dt* was calculated separately using each outline and then averaged.

Glacierwide *dV/dt* was converted to mass change rates using a density conversion factor (ρ) of 850 ± 60 kg m^{-3}, following Huss (2013). The mean specific mass-balance rate $\dot{B}$ (m w.e. yr^{-1}) was calculated by dividing the volume change rate by a representative glacier area ($\bar{A}$):

$$\dot{B} = \frac{\rho}{\rho_w} \frac{dV/dt}{\bar{A}}, \quad (3)$$

where ρ_w is the water density (1000 kg m^{-3}), and $\bar{A}$ is the representative glacier area (m^2). For eastern glaciers, $\bar{A}$ was calculated as the duration-weighted mean area derived from all available 2001–2019 outlines, whereas for western glaciers, it was calculated as the mean of the 1988 and 2019 glacier areas. One western glacier that was present in 1988 but had disappeared by 2019 was excluded from the glacier-specific and regional calculations.

The uncertainties for mass-balance estimates were from *dV/dt* calculation (σ_V), the representative area calculation (σ_{area}), and uncertainty in the density conversion factor (σ_ρ = 60 kg m^{-3}).

The uncertainties of *dV/dt* included DEM uncertainty ($\sigma_{V,DEM}$) and glacier outline uncertainty ($\sigma_{V,outline}$). For each glacier, these uncertainties were assumed to be independent and total *dV/dt* uncertainty (σ_V) was calculated as:

$$\sigma_V = \sqrt{\sigma_{V,DEM}^2 + \sigma_{V,outline}^2}, \quad (4)$$

DEM uncertainty was estimated from stable-terrain residuals using the H2022 workflow implemented in xDEM (Hugonnet et al., 2022; xDEM contributors, 2026). Spatially variable 1σ elevation errors were modelled as a function of terrain slope and maximum curvature. Spatial correlation in the residual errors was characterized using a two-scale variogram with Gaussian and spherical components. The resulting elevation error in each pixel was then converted to *dh/dt* uncertainty and were spatially propagated to *dV/dt* uncertainties for each glacier outline. The outline-specific DEM uncertainties were then combined in quadrature using the same temporal weights applied to the corresponding *dV/dt*.

https://doi.org/10.5194/egusphere-2026-7134
Preprint. Discussion started: 26 November 2026
© Author(s) 2026. CC BY 4.0 License.

For glacier outline uncertainty, the inward and outward buffered outlines represented the minimum and maximum glacier extents. Each buffered outline was used to extract *dh/dt* and calculate *dV/dt*. For each outline, half the absolute difference between the *dV/dt* estimates from the outward and inward buffers was taken as the uncertainty. These outline specific uncertainties were combined in quadrature using the same temporal weights approach. For western glaciers, half the absolute difference between the *dV/dt* estimates obtained from the 1988 and 2019 outlines was also included in quadrature as an additional geometry uncertainty.

The representative area ($\bar{A}$) uncertainty (σ_{area}) was derived from the inward and outward buffered outlines. For eastern glaciers, the uncertainties of the individual outlines were propagated using the same temporal weights. For western glaciers, the uncertainties of the 1988 and 2019 glacier area were combined in quadrature and divided by two to obtain the uncertainty in their mean.

Assuming that uncertainties of σ_V, σ_{area}, and σ_ρ were independent, the uncertainty in mass balance ($\sigma_{\dot{B}}$) was calculated as:

$$\sigma_{\dot{B}} = \sqrt{\left(\frac{\rho}{\rho_w}\frac{\sigma V}{\bar{A}}\right)^2 + \left(\frac{\rho(dV/dt)}{\rho_w \bar{A}^2}\sigma_{area}\right)^2 + \left(\frac{dV/dt}{\rho_w \bar{A}}\sigma_\rho\right)^2}, \quad (5)$$

Regional (eastern, western, and island-wide) mass change rates were calculated by summing the glacier-specific mass change rates (The GlaMBIE Team, 2025). Regional specific mass balance was calculated by dividing the summed mass change rate by the total representative glacier area. Regional DEM uncertainty was propagated over the union of the glaciers using the fitted spatial covariance model. Glacier outline and representative area uncertainties were combined in quadrature across glaciers, and all uncertainties were propagated to the regional specific mass-balance uncertainty. All uncertainties are reported as ± 1σ.

3.3 Ice thickness

We simulated ice thickness across Heard Island for 1947, 1988, and 2019, and for the eastern glaciers in 2001, using the GlabTop2 approach of Frey et al. (2014), implemented in GlabTop2-py v2.1.1 (Terink, 2024). GlabTop2 is a grid-based ice-thickness inversion model (Frey et al., 2014). It estimates ice thickness from glacier surface slope and basal shear stress based on the perfect-plasticity approximation:

$$H = \frac{\tau}{f\rho_i g \sin\alpha}, \quad (6)$$

where H (m) is ice thickness, τ (kPa) is the basal shear stress, f is a dimensionless valley-shape factor (0.8), ρ_i is ice density (900 kg m^{-3}), g is gravitational acceleration (9.81 m s^{-2}), and α is glacier surface slope.

The basal shear stress (τ) for each glacier and each reconstruction year is parameterized as a function of the elevation range following Haeberli and Hoelzle (1995) and Frey et al. (2014):

$$\tau = \begin{cases} 0.5 + 159.81\Delta Z - 43.5\Delta Z^2, & (\Delta Z \le 1.6\ km) \\ 150, & (\Delta Z > 1.6\ km) \end{cases}, \quad (7)$$

where ΔZ (km) is the glacier elevation range, defined as the difference between the maximum (Z_{max}; km) and minimum (Z_{min}; km) surface elevations within each glacier.

Local surface slope was calculated using the GlabTop2 adaptive-neighbourhood procedure (Frey et al., 2014). For each glacier, 30 % of the interior cells were randomly sampled, and the neighbourhood around each sampled cell was expanded from 3 × 3 cells until its elevation range reached 5 % of the glacier elevation range. Ice thickness was calculated from the resulting mean slope. The calculated ice thicknesses were then interpolated across each glacier, with a boundary constraint of 0 m along the glacier margins. Three random realizations were averaged to obtain the final thickness grid.

All calculations were performed on a 20 m grid. Island-wide ice thickness in 1947 and 1988 was reconstructed using the 1947 and 1988 glacier inventory, and the 2000 NASADEM. Gaps in NASADEM were filled using ASTER GDEM V3 (Fig. S2a).

https://doi.org/10.5194/egusphere-2026-7134
Preprint. Discussion started: 26 November 2026
© Author(s) 2026. CC BY 4.0 License.

Ice thickness for the six eastern glacier units in 2001 was reconstructed using the 2001 glacier outlines and the 2000 gap-filled NASADEM surface. Island-wide ice thickness in 2019 was reconstructed using the 2019 glacier inventory and the 2018-2019 Pléiades DEM. Gaps within the Pléiades DEM coverage were filled using the Copernicus DEM GLO-30 (Fig. S2b).
The temporal mismatch between the 2000 NASADEM and the 1947 and 1988 glacier outlines introduce additional uncertainty into the reconstructed ice thickness, particularly for the rapidly changing eastern glaciers. Owing to the limited observational availability, these datasets represent the closest available constraints.
Parameter sensitivity was assessed by varying the shape factor ($f = 0.8$) by ± 0.1 and the calculated glacier-specific τ by ± 20 %, following previous GlabTop2 sensitivity analyses (Frey et al., 2014), resulting in nine parameter combinations. Pixel-scale ice thickness uncertainty was calculated as the standard deviation (σ) of the nine modelled ice-thickness values.

3.4 Glacier volume and volume changes from inverted ice thicknesses

Glacier volumes in 1947, 1988, 2001, and 2019 were calculated from the inverted ice thicknesses described in Sect. 3.3. Uncertainty in glacier volume was estimated as the standard deviation across the nine parameter sensitivity experiments. Volume changes were calculated for all glaciers over the periods 1947–1988, and 1988–2019. For the eastern glaciers, additional volume changes were calculated for 2001–2019 using the 2001 ice thickness. This approach extended estimates of glacier volume change back to periods before suitable remote-sensing-derived DEMs were available for DEM differencing. Furthermore, ice thickness inversion enables us to estimate volume changes below the water level at lagoon-terminating glacier fronts, which are only partly captured by the DEM differencing approach (Hock et al., 2026).

4 Results

4.1 Glacier area and area changes

The glacier area across Heard Island was 289.4 ± 5.6 km^2 in 1947 (Table 2), covering approximately 79 % of the reference island area of 368 km^2 (Geoscience Australia, 2026). A continuous glacier area loss was observed from 1947 onwards (Fig. 3a), exposing more land area. By 1988, glacier area had decreased to 260.3 ± 4.2 km^2, representing a loss of 10.1 ± 2.3 % at a rate of 0.25 ± 0.06 % yr^{-1}. From 1988 to 2019, glacier area loss accelerated to 0.43 ± 0.05 % yr^{-1}. By 2019, the total glacier area had declined to 225.7 ± 2.5 km^2, covering approximately 61 % of the reference island area.
At regional scale, glacier area loss was substantially greater in the eastern than in the western sector. Between 1947 and 1988, glacier area decreased by 21.9 ± 2.7 % in the eastern sector (i.e., a rate of 0.53 ± 0.07 % yr^{-1}), compared with 5.1 ± 2.4 % (i.e. a rate of 0.12 ± 0.06 % yr^{-1}) in the western sector. Area loss accelerated in both sectors after 1988, with relative rates increasing to approximately 1.8 and 2.0 times their 1947-1988 values in the eastern and western sectors, respectively. This acceleration was particularly pronounced in the eastern sector after 2001, where the area loss rate increased from 0.51 ± 0.04 % yr^{-1} during 1947–2001 to 1.39 ± 0.12 % yr^{-1} during 2001–2019, approximately 2.7 times the earlier rate.
All five eastern glaciers examined in detail experienced substantial area loss between 2001 and 2019, although their magnitudes and temporal patterns differed (Fig. 3b). Stephenson Glacier showed the largest reduction, decreasing from 21.1 ± 0.5 km^2 in 2001 to 11.7 ± 0.2 km^2 in 2019, corresponding to an area loss of 44.6 ± 1.7 % (Table 2). Its area loss rate was −2.48 ± 0.09 % yr^{-1}, approximately 1.8 times that of the eastern sector. Much of this reduction occurred before 2010, by which time Stephenson Glacier had already lost 33.9 ± 2.4 % of its 2001 area.
When Stephenson Glacier was excluded, the combined area of the remaining eastern glaciers decreased by 14.8 ± 2.8 % between 2001 and 2019, corresponding to an average relative area loss rate of 0.82 ± 0.16 % yr^{-1}. Specifically, Brown, G073625E53121S, and Winston Glaciers experienced area losses of 19.0 ± 3.7 %, 17.1 ± 3.3 %, and 16.0 ± 3.1 %, respectively, between 2001 and 2019. Compton Glacier experienced the smallest relative area loss, remaining nearly stable between 2001 and 2010 before losing 11.6 ± 3.3 % of its 2001 area by 2019.

https://doi.org/10.5194/egusphere-2026-7134
Preprint. Discussion started: 26 November 2026
© Author(s) 2026. CC BY 4.0 License.

Table 2. Glacier area and relative area changes for Heard Island from 1947 to 2019. All uncertainties are reported as 1σ.

Region	Area (km^2)				Relative area change (%)			Relative area change rate (% yr^{-1})		
	1947	1988	2001	2019	1947-1988	1988-2019	2001-2019	1947-1988	1988-2019	2001-2019
Heard Island	289.4 ± 5.6	260.3 ± 4.2	--	225.7 ± 2.5	−10.1 ± 2.3	−13.3 ± 1.7	--	−0.25 ± 0.06	−0.43 ± 0.05	--
Western Sector	204.3 ± 4.3	193.9 ± 2.9	--	179.3 ± 1.8	−5.1 ± 2.4	−7.5 ± 1.7	--	−0.12 ± 0.06	−0.24 ± 0.05	--
Eastern Sector	85.1 ± 2.0	66.5 ± 1.7	61.8 ± 1.2	46.3 ± 0.9	−21.9 ± 2.7	−30.3 ± 2.2	−25.0 ± 2.1	−0.53 ± 0.07	−0.98 ± 0.07	−1.39 ± 0.12
Stephenson Glacier	30.8 ± 1.0	24.2 ± 0.7	21.1 ± 0.5	11.7 ± 0.2	−21.3 ± 3.4	−51.9 ± 1.6	−44.6 ± 1.7	−0.52 ± 0.08	−1.67 ± 0.05	−2.48 ± 0.09

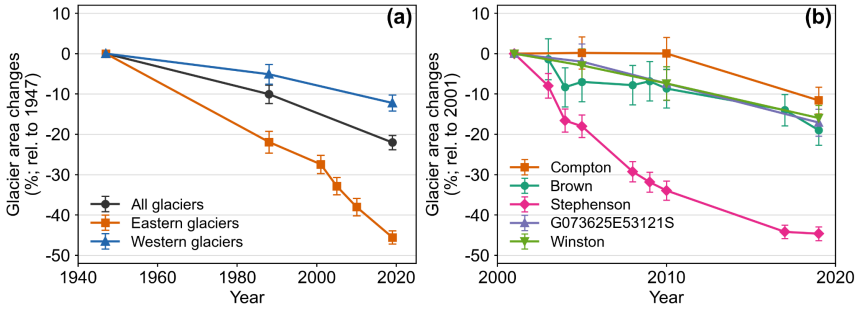

Figure 3. Relative area changes for **(a)** all glaciers, the eastern and the western glaciers from 1947 to 2019, and for **(b)** several eastern glaciers from 2001 to 2019. Error bars indicate 1σ uncertainties, calculated by propagating the independent buffer-derived mapping uncertainties of the inventories.

4.2 Glacier volume and mass changes by DEM differencing

Pixel-based glacier elevation-change rates averaged over 2000−2019 across Heard Island (Fig. 4a), ranging from −11.77 to +5.71 m yr^{-1}, with a median of −0.27 m yr^{-1}. Approximately 24 % of the pixels had positive elevation-change rates mainly at higher elevations within the glacier accumulation zones. Surface lowering was concentrated mainly near glacier termini and was particularly marked on the eastern glaciers.

Based on the glacier elevation-change rates and glacier areas, glacier volume changes were calculated for 2000−2019. Over this period, Heard Island experienced a total glacier volume loss of 1.6 ± 0.0 km^3. The eastern sector accounted for 0.7 ± 0.0 km^3 (44 %) of the total loss, while the western sector accounted for the rest.

Resulting glacier-wide mass balances ranged from −1.10 ± 0.08 to +0.28 ± 0.28 m w.e. yr^{-1} (Fig. 4B; Table S1). The most positive value occurred for a very small glacier (No. 24) within the Laurens Peninsula ice complex, although it was not statistically distinguishable from zero. Given its small size and observed recession, this positive estimate likely reflects uncertainty rather than sustained glacier mass gain. Particularly strong specific mass losses were found at Stephenson (−1.10 ± 0.08 m w.e. yr^{-1}) and Brown (−0.72 ± 0.05 m w.e. yr^{-1}) glaciers, consistent with their large observed glacier area losses.

At the regional scales, the specific mass balance was −0.28 ± 0.02 m w.e. yr^{-1} for Heard Island, −0.53 ± 0.04 m w.e. yr^{-1} for the eastern glaciers, and −0.21 ± 0.02 m w.e. yr^{-1} for the western glaciers.

https://doi.org/10.5194/egusphere-2026-7134
Preprint. Discussion started: 26 November 2026
© Author(s) 2026. CC BY 4.0 License.

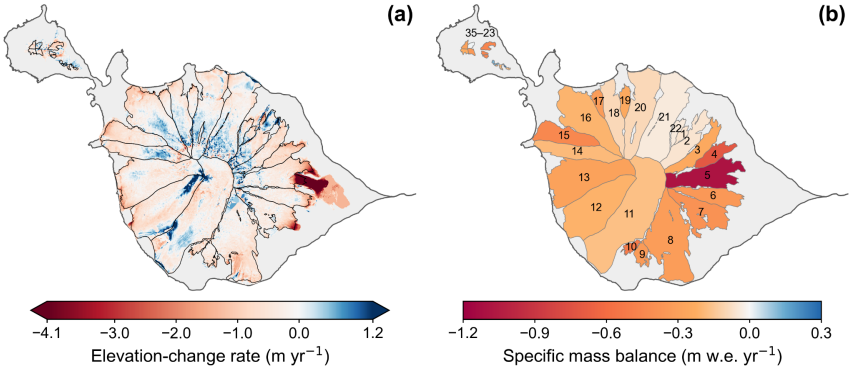

Figure 4. (a) Island-wide spatial distribution of surface elevation-change rates derived from the 2000 NASADEM and 2019 Pléiades DEM. The exact DEM acquisition dates are provided in Fig. S1. The colour bar range is capped at approximately the 99th percentile. **(b)** Glacierwide specific mass balances derived from the same DEM difference and displayed using the 2019 glacier outlines.

4.3 Spatial distribution of simulated ice thickness

The spatial distribution of inverted ice thickness from 1947 to 2019 is shown in Fig. 5. Ice thickness was highly heterogeneous across Heard Island, with thicker ice mainly occurring within the broad, low-gradient terminal regions of several large glaciers, including Stephenson, Vahsel, Downes, and Ealey Glaciers. Locally thick ice was also present around Big Ben, extending outward into several major glacier valleys. In contrast, relatively thin ice was found along glacier margins, on steeper slopes, and within the smaller glaciers on Laurens Peninsula. This spatial pattern was evident across all reconstructed periods, although thicker ice in the terminal and lower reaches of glaciers progressively became less extensive through time.

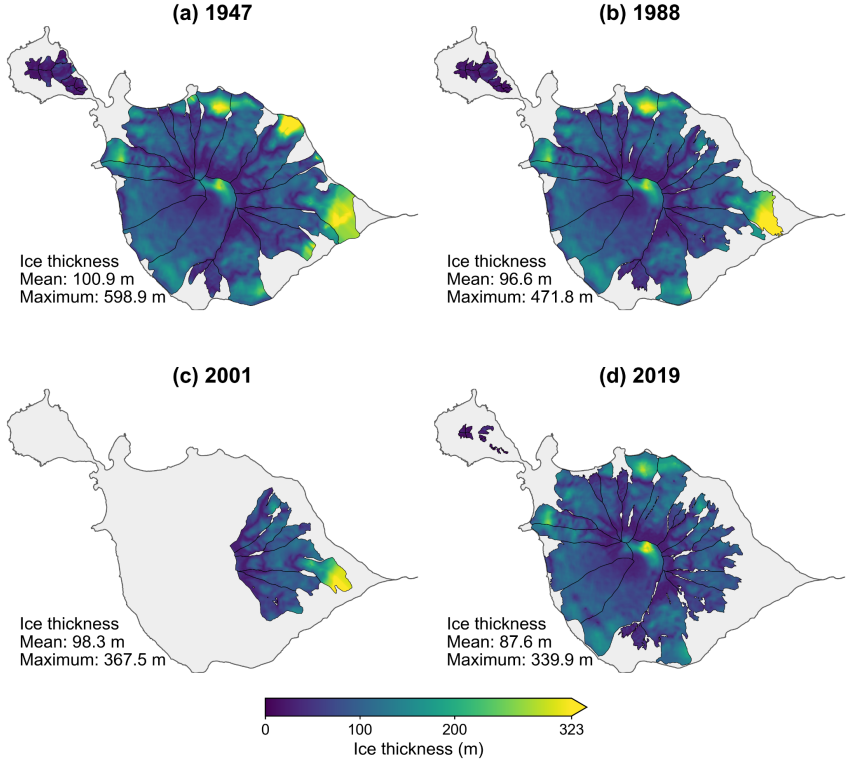

Figure 5. Spatial distribution of reconstructed ice thickness for **(a)** all glaciers in 1947, **(b)** all glaciers in 1988, **(c)** the eastern glaciers in 2001, and **(d)** all glaciers in 2019. A common colour scale was applied to all panels, with its upper limit set to the 99th percentile of the 1947 ice thickness to reduce the visual influence of isolated extreme values.

https://doi.org/10.5194/egusphere-2026-7134
Preprint. Discussion started: 26 November 2026
© Author(s) 2026. CC BY 4.0 License.

Glacier recession resulted in the loss of ice from the thick terminal areas, accompanied by an overall decrease in mean ice thickness. Across Heard Island, mean ice thickness decreased from 100.9 ± 20.9 m in 1947 to 87.6 ± 18.2 m in 2019, representing a reduction of 13.3 ± 2.8 m. This decrease was particularly pronounced in the eastern sector, where glacier recession was more rapid than in the western sector (Fig. 3). Mean ice thickness in the eastern glaciers decreased from 123.1 ± 25.6 m in 1947 to 98.3 ± 20.4 m in 2001, corresponding to a reduction of 24.7 ± 5.1 m, and subsequently decreased by a further 22.2 ± 4.6 m to 76.1 ± 15.8 m in 2019.

4.4 Glacier volume and volume changes from inverted ice thicknesses

Changes in the ice thickness indicate a continuous glacier volume loss across Heard Island between 1947 and 2019 (Table 3). Total glacier volume decreased from 29.2 ± 6.1 km^3 in 1947 to 25.2 ± 5.2 km^3 in 1988, corresponding to a loss of 4.0 ± 0.8 km^3 and to a relative loss rate of 0.34 ± 0.07 % yr^{-1}. Volume loss accelerated after 1988 (0.69 ± 0.14 % yr^{-1}), with glacier volume decreasing by a further loss of 5.4 ± 1.1 km^3.

The eastern glaciers contributed most of the total volume loss across Heard Island. Between 1947 and 2019, the eastern sector lost 6.9 ± 1.4 km^3 of ice, accounting for 74 % of the island-wide loss, compared with 26 % from the western sector. Relative volume loss rates also differed markedly between the two sectors and accelerated after 1988 in both regions. In the eastern sector, the rate increased from 0.76 ± 0.16 % yr^{-1} during 1947–1988 to 1.65 ± 0.34 % yr^{-1} during 1988–2019, while in the western sector it increased from 0.10 ± 0.02 to 0.31 ± 0.06 % yr^{-1}.

A large proportion of the eastern-sector volume loss was associated with Stephenson Glacier, especially during 1988–2019. Over this period, it lost 3.0 ± 0.6 km^3 of ice and accounted for 80 % of the eastern-sector volume loss and 55 % of the island-wide volume loss. This dominance persisted during the more recent 2001–2019 period, when Stephenson Glacier lost 2.0 ± 0.4 km^3 of ice and again accounted for 80 % of the total eastern-sector volume loss. However, its relative volume loss rate increased to 3.85 ± 0.80 % yr^{-1} during 2001–2019, compared with 2.47 ± 0.51 % yr^{-1} over 1988–2019, indicating an acceleration after 2001.

Table 3. Glacier volume and volume changes for Heard Island during 1947–2019 from inverted ice thicknesses. All uncertainties are reported as 1σ.

Region	Volume (km^3)				Volume change (km^3)			Relative volume change rate (% yr^{-1})		
	1947	1988	2001	2019	1947-1988	1988-2019	2001-2019	1947-1988	1988-2019	2001-2019
Heard Island	29.2 ± 6.1	25.2 ± 5.2	--	19.8 ± 4.1	−4.0 ± 0.8	−5.4 ± 1.1	--	−0.34 ± 0.07	−0.69 ± 0.14	--
Western Sector	18.7 ± 3.9	17.9 ± 3.7	--	16.2 ± 3.4	−0.8 ± 0.2	−1.7 ± 0.4	--	−0.10 ± 0.02	−0.31 ± 0.06	--
Eastern Sector	10.5 ± 2.2	7.2 ± 1.5	6.1 ± 1.3	3.5 ± 0.7	−3.2 ± 0.7	−3.7 ± 0.8	−2.5 ± 0.5	−0.76 ± 0.16	−1.65 ± 0.34	−2.33 ± 0.48
Stephenson Glacier	4.8 ± 1.0	3.9 ± 0.8	2.9 ± 0.6	0.9 ± 0.2	−0.9 ± 0.2	−3.0 ± 0.6	−2.0 ± 0.4	−0.48 ± 0.10	−2.47 ± 0.51	−3.85 ± 0.80

5 Discussion

5.1 Comparison with global products

This section evaluates the consistency and discrepancy of our glacier mass-balance, ice thickness, and volume estimates with available global products (Hugonnet et al., 2021; WGMS, 2026; Farinotti et al., 2019; Millan et al., 2022; Frank et al., 2026; Maffezzoli et al., 2026) at island-wide, regional, and glacier-specific scales (Table 4). Attention is given to potential causes of these differences, including variations in input data, temporal and spatial coverage, and methodological assumptions.

https://doi.org/10.5194/egusphere-2026-7134
Preprint. Discussion started: 26 November 2026
© Author(s) 2026. CC BY 4.0 License.

Table 4. Glacier average mass-balance estimates from 2000-2019 and glacier volume estimates in 1988 for Heard Island, compared with the results from global products. All uncertainties are reported as 1σ.

Region	Mass balance (m w.e. yr^{-1})			1988 glacier volume (km^3)				
	This study	Hugonnet et al. (2021) [1]	WGMS (2026) [2]	This study	Farinotti et al. (2019)	Millan et al. (2022)	Frank et al. (2026)	Maffezzoli et al. (2026)
Heard Island	−0.28 ± 0.02	−0.28 ± 0.14	−0.18 ± 0.49	25.2 ± 5.2	23.5 ± 6.1	25.4 ± 10.7	28.0 ± 4.6	36.8 ± 10.0
Western Sector	−0.21 ± 0.02	−0.19 ± 0.15	−0.04 ± 0.48	17.9 ± 3.7	16.8 ± 4.4	19.3 ± 8.1	22.4 ± 3.7	27.8 ± 7.6
Eastern Sector	−0.53 ± 0.04	−0.53 ± 0.11	−0.59 ± 0.51	7.2 ± 1.5	6.7 ± 1.7	6.1 ± 2.6	5.6 ± 0.9	9.1 ± 2.4
Stephenson Glacier	−1.10 ± 0.08	−1.44 ± 0.11	−1.41 ± 0.52	3.9 ± 0.8	3.7 ± 1.0	2.9 ± 1.1	2.0 ± 0.3	4.3 ± 1.0

[1] For Hugonnet et al. (2021), we extract the average "*dmdtda*" estimates for the period from 1 January 2000 to 1 January 2020. The original uncertainties are reported at the 95 % confidence level (1.96σ) and are converted to 1σ uncertainties by dividing by 1.96.
[2] For WGMS (2026), we calculate the arithmetic mean of the 20 annual mass-balance estimates and annual total uncertainties (1σ) from 2000 to 2019 for each glacier.

5.1.1 Mass balance comparisons

All products indicate a negative island-wide mass balance, although the estimated magnitudes differ (Table 4). The estimate from Hugonnet et al. (2021), −0.28 ± 0.14 m w.e. yr^{-1}, is nearly identical to our estimate of −0.29 ± 0.02 m w.e. yr^{-1}. WGMS (2026) produces a less negative island-wide estimate of −0.18 ± 0.49 m w.e. yr^{-1}. Agreement is particularly strong for the eastern glaciers. In contrast, the global products indicate weaker mass loss for the western glaciers, especially from WGMS (2026).

The two global products show highly heterogeneous mass-balance patterns across Heard Island, with positive and negative estimates interspersed without a clear spatial pattern (Fig. 6). By comparison, the estimates obtained in this study show a clearer and more regionally coherent spatial distribution, particularly over western Heard Island (Fig. 4b).

Specifically, Hugonnet et al. (2021) exhibited the widest range, from −2.80 ± 1.12 to +6.67 ± 0.85 m w.e. yr^{-1}. The most negative estimate occurred for RGI60-19.01696, corresponding mainly to unnamed western glacier No. 17, for which this study estimated −0.33 ± 0.04 m w.e. yr^{-1}. The maximum positive estimate occurs among the small glaciers on Laurens Peninsula. WGMS (2026) exhibits a narrower range, from −1.41 ± 0.52 to +1.16 ± 0.51 m w.e. yr^{-1}. Its most negative estimate occurs for Stephenson Glacier, for which this study yielded −1.10 ± 0.08 m w.e. yr^{-1}.

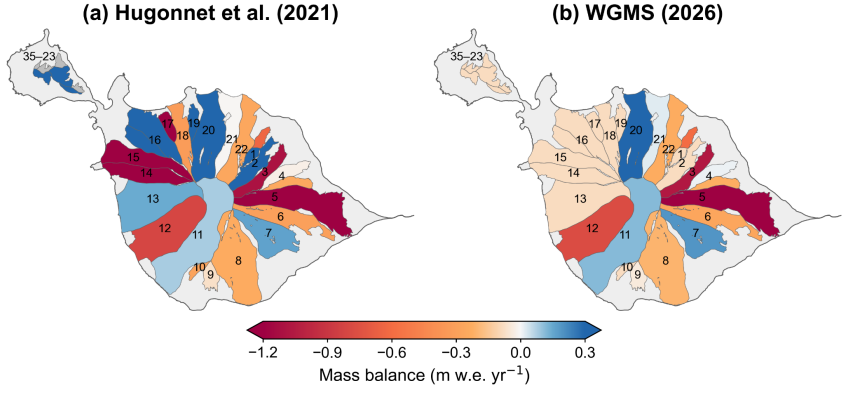

Figure 6. Spatial distribution of glacier-specific mass-balance estimates for 2000–2019 from **(a)** Hugonnet et al. (2021) and **(b)** WGMS (2026). Values are displayed using the 1988 RGI 6.0 glacier outlines. Grey glacier polygons in **(a)** indicates missing data. Both panels use the same colour scale as Fig. 4b. Glacier numbers correspond to the 2019 glacier inventory shown in Fig. 1.

The sources of the differences between our estimates and the global products are difficult to isolate because the estimates are derived using different approaches and standards (Hock et al., 2026). Nevertheless, some inferences can still be drawn from the limited available information. One of the most important potential explanations is the large number of spatial gaps in the *dh/dt* data of Hugonnet et al. (2021) over Heard Island, especially within the western sectors and peak regions on Big Ben (Fig.

https://doi.org/10.5194/egusphere-2026-7134
Preprint. Discussion started: 26 November 2026
© Author(s) 2026. CC BY 4.0 License.

S3a). Hugonnet et al. (2021) used multi-temporal ASTER DEMs acquired between 1 January 2000 and 1 January 2020 to estimate *dh/dt*. However, the persistent cloud cover over Heard Island likely limited the availability of suitable ASTER imagery (Tielidze et al., 2025).

A second potential source of discrepancy is the different spatial distribution of *dh/dt* between the two datasets (Fig. S3b). Compared with our results, more positive *dh/dt* in Hugonnet et al. (2021) occurs mainly at middle elevations, whereas our positive *dh/dt* values are generally found at higher elevations (Fig. S4). Hugonnet et al. (2021) also shows stronger surface lowering near several glacier termini. These differences may partly offset each other at the glacier scale for the eastern glaciers but may have a greater influence on the western glaciers, where *dh/dt* data are extensively missing near the termini.

An additional source of discrepancy is deviations from full mass-balance years. Even differences of a few weeks in DEM acquisition dates can introduce large biases in mass-balance estimates (Yang et al., 2020; Hock et al., 2026). Hugonnet et al. (2021) used multi-temporal DEMs to reconstruct elevation-change time series, which may partially reduce the influence of different DEM acquisition dates. However, seasonal biases may still affect the estimates, particularly for DEM pairs acquired in different seasons. In our study, the limited availability of suitable DEMs makes it difficult to account for these seasonal differences (Fig. S1).

A fourth potential source of discrepancy is the temporal inconsistency between the glacier outlines and the mass-balance period used by Hugonnet et al. (2021). For Heard Island, the RGI 6.0 glacier outlines are dated to 1988, whereas the reported mass balances cover 2000–2020. Our sensitivity experiments show that using different glacier inventories can produce mass-balance estimates in eastern Heard Island ranging from −0.39 to −0.61 m w.e. yr^{-1}, compared with the reference value of −0.54 m w.e. yr^{-1}, corresponding to differences of approximately 14–28 % (Fig. 7). This effect is especially pronounced for rapidly retreating glaciers (Hock et al., 2026). For Stephenson Glacier, the mass balance is −1.10 m w.e. yr^{-1}, while the sensitivity experiments yield values ranging from −0.64 to −1.23 m w.e. yr^{-1}, corresponding to differences of approximately 12–41%.

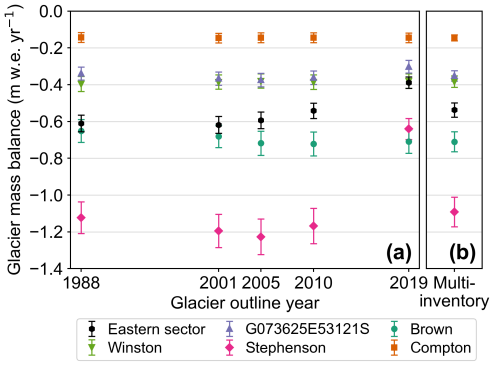

Figure 7. Glacierwide mass-balance estimates for the eastern sector and individual eastern glaciers over the period 2000-2019. **(a)** using only one-year glacier outline (1988, 2001, 2005, 2010, and 2019, respectively) to extract *dh/dt* and calculate glacier area, and **(b)** using multiple glacier inventories and the duration-weighting approach described in Sect. 3.3. Error bars represent 1σ uncertainties.

The integration of long-term glaciological observations in the annual global product (WGMS, 2026; Dussaillant et al., 2025; The WGMS Network, 2026) appears to provide some correction to the mass-balance estimates derived from DEM differencing by Hugonnet et al. (2021). It reduces some of the positive mass-balance estimates for western glaciers (Fig. 6) that are inconsistent with the observed glacier recession on the island (Tielidze et al., 2025). Nevertheless, the temporal consistent mass-balance estimates derived from DEM differencing remain a fundamental basis for Heard Island assessments, as scientific visits to the island typically only occur every few decades and thus in situ glaciological observations are limited.

https://doi.org/10.5194/egusphere-2026-7134
Preprint. Discussion started: 26 November 2026
© Author(s) 2026. CC BY 4.0 License.

5.1.2 Ice thickness and glacier volume comparisons

Temporal inconsistency remained in the ice thickness inversion and glacier volume estimates. Although the 2019 Heard Island and 2001 eastern-sector calculations were broadly consistent in the timing of the DEMs and glacier outlines in this study, the use of the 2000 NASADEM with the 1947 and 1988 glacier outlines introduced additional uncertainty into the earlier estimates. Similar temporal inconsistencies are present in global ice thickness products, where glacier outlines, DEMs, and other observational constraints often represent different period (Farinotti et al., 2019; Millan et al., 2022; Frank et al., 2026; Maffezzoli et al., 2026). For example, the RGI glacier outlines for Heard Island represent 1988 (RGI Consortium, 2017, 2023), whereas the DEM and other observational constraints used in global ice thickness products represent later periods. These include surface topography around 2000 in Farinotti et al. (2019), ice velocities from 2017–2018 in Millan et al. (2022), Copernicus DEM surface elevations representing mainly 2011–2015 in Frank et al. (2026), and TanDEM-X surface elevations from 2010–2014 in Maffezzoli et al. (2026).

To enable a more consistent comparison among our results and the global products, we focused on the 1988 ice volume (Table 4; Fig. 8). At the island scale, most global estimates were broadly consistent with our glacier volume results, with differences generally within about 10 %, except for Maffezzoli et al. (2026). Maffezzoli et al. (2026) produced a substantially higher estimate of 36.8 ± 10.0 km^3, compared with 25.2 ± 5.2 km^3 in this study. Larger discrepancies emerged at the regional scale, particularly in the western sector, where several global products estimated greater glacier volumes than our results.

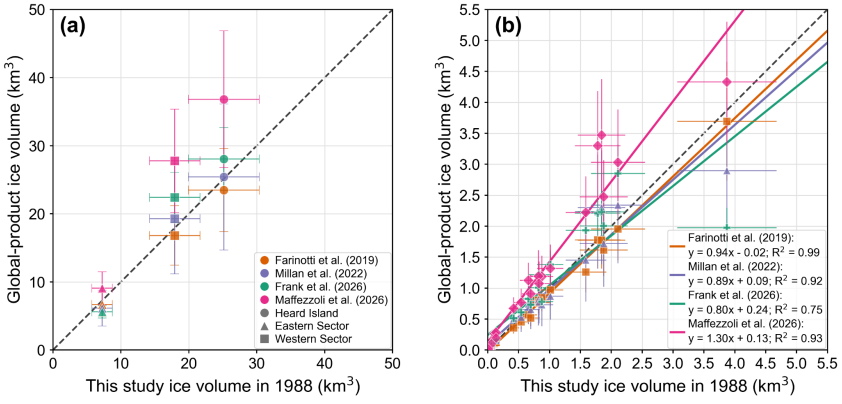

Figure 8. Comparison of glacier volumes reconstructed for 1988. **(a)** Island-wide, eastern-sector, and western-sector glacier volumes reconstructed in this study are compared with estimates from Farinotti et al. (2019), Millan et al. (2022), Frank et al. (2026), and Maffezzoli et al. (2026). **(b)** Glacier-specific volumes for the 22 glacier units with a unique one-to-one correspondence between the Tielidze et al. (2025) inventory and the RGI inventories. Error bars represent 1σ uncertainties, coloured solid lines show linear regressions, and the dashed lines indicate 1:1 agreement.

At the glacier scale (Fig. 8b), glacier units in the RGI inventories do not correspond exactly to those in the 1988 inventory of Tielidze et al. (2025). We therefore restrict the glacier-specific comparison to the 22 glacier units for which a unique one-to-one correspondence with a single RGI ID could be established. The estimates from Farinotti et al. (2019) and Millan et al. (2022) show the closest agreement with our study. In contrast, Maffezzoli et al. (2026) generally estimates larger glacier volumes, as indicated by a regression slope of 1.30. Frank et al. (2026) shows a weaker relationship, with a slope of 0.80 and an R^2 of 0.75. This weaker fit is strongly influenced by substantial data gaps over Stephenson Glacier (Fig. S5), which has the largest reconstructed volume among the 22 glaciers included in the comparison.

Differences between our reconstruction in 1988 and the four global datasets are a function of the methods and assumptions used to estimate ice thickness and glacier volume. The relatively small differences between our reconstructions and those of Farinotti et al. (2019) and Millan et al. (2022) may be partly because all three datasets are based on the shallow-ice approximation (SIA) or perfect-plasticity assumption. The reconstructed ice thickness is strongly constrained by surface

https://doi.org/10.5194/egusphere-2026-7134
Preprint. Discussion started: 26 November 2026
© Author(s) 2026. CC BY 4.0 License.

topography and glacier geometry. In contrast, Maffezzoli et al. (2026) and Frank et al. (2026) applied machine-learning and higher-order ice-flow approaches, respectively, which may help explain the larger differences from our estimates.

The spatial pattern of our ice thickness estimates is broadly consistent with that of the global ice thickness products, with thicker ice concentrated mainly near the termini of several large glaciers and around Big Ben (Fig. S5). However, the maximum ice thickness and mean ice thickness differed among the datasets. In the SIA-based products of Farinotti et al. (2019) and Millan et al. (2022), the greatest thickness occurred at the terminus of Stephenson Glacier and reached approximately 550–770 m. Our estimate was intermediate, with a maximum thickness of about 470 m, while the maximum values in Frank et al. (2026) and Maffezzoli et al (2026) were lower, at around 420 m.

All ice thickness estimates show relatively thick ice at the terminus of Stephenson Glacier compared with the available bathymetric observations (Fig. S6 and Fig. S7). The bathymetric survey conducted between 21 January and 15 February 2004 provided direct constraints on the bed elevation within the lagoons (Donoghue, 2009). The surveyed bed elevations indicate substantially shallower water depth than those inferred from the NASADEM and the ice thickness products near the glacier terminus by roughly 100–300 m (Fig. S7), suggesting that ice thickness in this region may be overestimated.

When the 2000 NASADEM is combined with the 1988 glacier outline, parts of the former glacier terminus that are occupied by the lagoon are represented by surface elevations close to 0 m. This produces an unrealistic surface geometry and modifies the glacier surface slopes within the historical glacier extent. The temporal inconsistency between DEMs and glacier outlines may have a larger influence on SIA-based ice thickness estimates (Fig. S7). Because SIA-based ice thickness estimates are directly influenced by surface slope (Hutter, 1983; Morland, 1984; Zekollari et al., 2022), such temporal mismatches can propagate directly into the inferred ice thickness near the former terminus of Stephenson Glacier.

5.2 Spatiotemporal pattern of glacier change on Heard Island

Our results and previous study (Tielidze et al., 2025) show that glacier change on Heard Island has spatially heterogeneous and has accelerated over time. To facilitate comparison between the earlier and more recent periods, glacier area and volume changes were standardized to the 1947–2000 and 2000–2019 periods (Table 5). The mean annual change rates were calculated from all available observation intervals, and the corresponding changes were obtained by multiplying these rates by 53 and 19 years, respectively.

Table 5. Glacier changes standardized to the 1947–2000 and 2000–2019 periods.

Period	Variable	Heard Island	Western Sector	Eastern Sector	Stephenson Glacier
1947-2000	Area change (km^2)	-39.1 ± 5.2	-16.1 ± 4.7	-23.0 ± 2.3	-9.5 ± 1.1
	Area change rate ($km^2\ yr^{-1}$)	-0.74 ± 0.10	-0.30 ± 0.09	-0.43 ± 0.04	-0.18 ± 0.02
	Volume change (km^3) [1]	-5.8 ± 1.2	-1.5 ± 0.3	-4.3 ± 0.9	-1.8 ± 0.4
	Volume change rate ($km^3\ yr^{-1}$) [1]	-0.11 ± 0.02	-0.03 ± 0.01	-0.08 ± 0.02	-0.03 ± 0.01
2000-2019	Area change (km^2)	-24.7 ± 3.0	-8.9 ± 2.6	-15.8 ± 1.5	-9.6 ± 0.5
	Area change rate ($km^2\ yr^{-1}$)	-1.30 ± 0.16	-0.47 ± 0.14	-0.83 ± 0.08	-0.51 ± 0.03
	Volume change (km^3) [1]	-3.7 ± 0.8	-1.0 ± 0.2	-2.7 ± 0.6	-2.2 ± 0.7
	Volume change rate ($km^3\ yr^{-1}$) [1]	-0.20 ± 0.04	-0.05 ± 0.01	-0.14 ± 0.03	-0.12 ± 0.04
	Volume change (km^3) [2]	-1.6 ± 0.0	-0.9 ± 0.0	-0.7 ± 0.0	-0.4 ± 0.0
	Volume change rate ($km^3\ yr^{-1}$) [2]	-0.08 ± 0.00	-0.05 ± 0.00	-0.04 ± 0.00	-0.02 ± 0.00

[1] Glacier volume changes and change rates derived from ice thickness estimates.
[2] Glacier volume changes and change rates derived from DEM differencing.

5.2.1 Temporal changes and climatic controls

After standardization, glacier loss across Herad Island showed a clear acceleration after 2000 (Table 5). During 2000–2019, area and volume losses were both about 64 % of those accumulated over the much longer 1947–2000 period. The mean annual loss rates during 2000–2019 were 1.30 ± 0.16 $km^2\ yr^{-1}$ for glacier area and 0.20 ± 0.04 $km^3\ yr^{-1}$ for glacier volume, compared with 0.74 ± 0.10 $km^2\ yr^{-1}$ and 0.11 ± 0.02 $km^3\ yr^{-1}$, respectively, during the earlier period. Both rates were approximately 1.8 times those during the earlier period.

https://doi.org/10.5194/egusphere-2026-7134
Preprint. Discussion started: 26 November 2026
© Author(s) 2026. CC BY 4.0 License.

The accelerated glacier area and mass losses were driven largely by changes in temperature and precipitation. Over 1947–2019 period, both air temperature and precipitation increased across Heard Island (Fig. 9). Regional warming can affect glacier mass balance through multiple processes (Tielidze et al., 2025). The warming trend strengthened after 2000, increasing from about +0.01 °C yr^{-1} during 1947–2000 to around +0.03 °C yr^{-1} during 2000–2019 (Fig. 9a), likely enhancing surface melt. The accelerated regional warming was also associated with an increase in the number of days per year with mean air temperature above 0 °C, with an average of approximately 15 more days in ERA5 and 19 more days in ERA5-Land during 2000–2019 compared with the earlier period (Fig. 9c), prolonging the ablation season.

Increased precipitation may have enhanced accumulation and caused positive *dh/dt* (Fig. 4a) in the high accumulation regions. However, the proportion of precipitation falling as snow decreased, with mean snowfall fraction declining by approximately 4.7 and 3.9 % during 2000–2019 compared with the pre-2000 period in ERA5 and ERA5-Land, respectively (Fig. 9d), potentially reducing snow accumulation on the glaciers. Moreover, the increase in precipitation weakened after 2000 (Fig. 9b), while the warming trend intensified (Fig. 9a). This shift toward more rapid warming likely enhanced melt and contributed to more negative glacier mass balances, and to the acceleration of glacier area and mass losses.

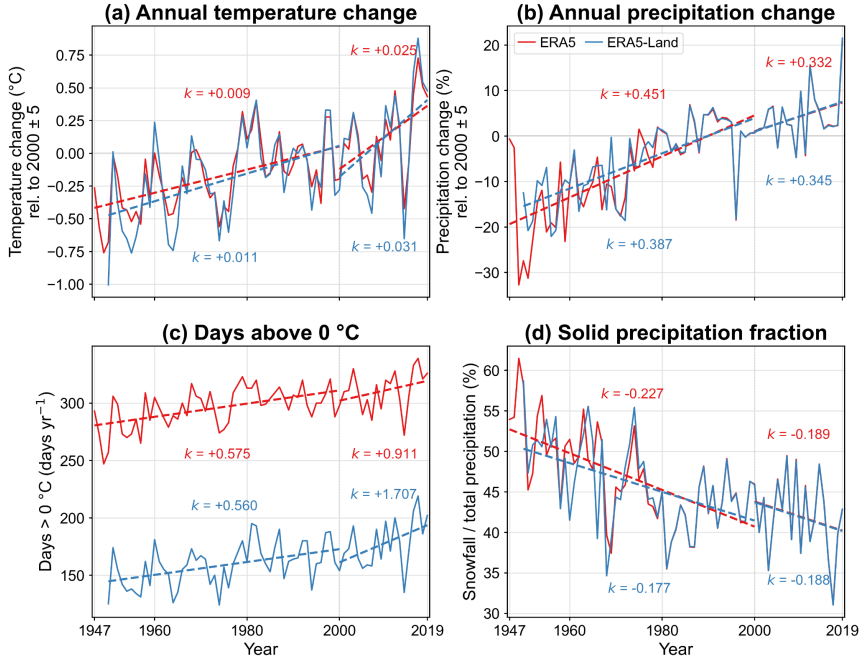

Figure 9. Annual variations in **(a)** 2 m air temperature, **(b)** total precipitation, **(c)** the number of days with daily mean 2 m air temperature above 0 °C, and **(d)** snowfall as a percentage of total precipitation over Heard Island, derived from ERA5 (Hersbach et al., 2020) and ERA5-Land (Muñoz-Sabater et al., 2021). Values in **(a)** and **(b)** are expressed relative to the 1995–2005 mean. ERA5 and ERA5-Land have horizontal resolutions of 0.25° and 0.10°, respectively. Differences in spatial resolution led to different mean temperature over Heard Island and a marked offset in the number of days above 0 °C. Solid lines show annual changes, while dashed lines show linear trends for 1947–2000 (ERA5) or 1950–2000 (ERA5-land) and 2000–2019. The *k* indicates the corresponding trend slopes.

Accelerated glacier loss has been widely observed at the global scale and across many regions of the Southern Hemisphere. Global observations since the 1960s show a progressive increase in glacier mass-loss rates, with acceleration during the 1990s and particularly strong losses in recent decades (Zemp et al., 2019; Hugonnet et al., 2021; The GlaMBIE Team, 2025). The persistence of this trend is supported by the WGMS global record, in which six of the highest annual glacier mass loss years since 1975 occurred within the most recent seven years (The WGMS Network, 2026).

Similar accelerations have been reported in several Southern Hemisphere glacierized regions. In the Southern Alps of New Zealand, the long-term rate of ice loss has nearly doubled relative to earlier periods (Carrivick et al., 2020). Across the Andes and Patagonia, high and locally accelerating glacier area and mass losses have also been documented, although the magnitude

https://doi.org/10.5194/egusphere-2026-7134
Preprint. Discussion started: 26 November 2026
© Author(s) 2026. CC BY 4.0 License.

and temporal evolution vary considerably among regions and individual glaciers (Dussaillant et al., 2019; Minowa et al., 2021; Carrivick et al., 2024).

On South Georgia, the average glacier recession rates increased from 8 m yr^{-1} in the 1950s to 35 m yr^{-1} at the beginning of the 21st century (Cook et al., 2010), with substantial glacier thinning and mass loss continuing between 2000 and 2013 (Farías-Barahona et al., 2020). On the Kerguelen Islands nearby Heard Island, glacier recession accelerated markedly after the early 1990s, with the area loss rate approximately doubling between 1963–1991 and 1991–2003 (Berthier et al., 2009), followed by continued rapid ice loss during the 2000s (Favier et al., 2016).

5.2.2 Spatial variations and potential controls

Glacier change across Heard Island was not spatially uniform, with larger area and volume losses in the eastern sector than in the western sector (Table 5). This contrast was particularly evident for several large eastern glaciers, especially Stephenson Glacier, which accounted for a large proportion of the total ice loss. Such spatial differences suggest that glacier response was influenced not only by the island-wide climatic forcing discussed above, but also by local controls.

We examine the potential controls on these spatial variations using mass-balance estimates, ice-thickness patterns, and glacier area and volume changes during 2000–2019, when the most comprehensive observational data are available. We then extend the interpretation to the full 1947–2019 period.

The mass-balance estimates during 2000–2019 show a pronounced east–west contrast, with the eastern glaciers experiencing a mass-loss rate approximately 2.5 times that of the western glaciers. However, the east–west classification adopted from Tielidze et al. (2025) masks substantial glacier-scale variability. The strongly negative eastern estimate is driven primarily by Stephenson and Brown Glaciers, with specific mass balances of -1.10 ± 0.08 and -0.72 ± 0.05 m w.e. yr^{-1}, respectively. For Brown Glacier, the delineation of ice divide excludes part of the upper accumulation areas where positive elevation changes are observed (Fig. 4a), which may bias the glacierwide mass-balance estimates to more negative values. Thus, the spatial heterogeneity in glacier change across Heard Island appears to be largely concentrated at Stephenson Glacier.

When Stephenson Glacier was excluded, the regional mass balance of the remaining five eastern glacier units was -0.32 ± 0.03 m w.e. yr^{-1}. The corresponding value for the remaining 28 glacier units across Heard Island was -0.23 ± 0.02 m w.e. yr^{-1}, close to the western-sector estimate of -0.21 ± 0.02 m w.e. yr^{-1}. This indicates that the apparent east–west contrast of glacier mass balance during 2000–2019 is strongly influenced by the exceptional mass loss of Stephenson Glacier rather than reflecting a uniform difference between all eastern and western glaciers.

The comparison between glacier volume changes derived from ice thickness estimates and DEM differencing further highlights the exceptional behaviour of Stephenson Glacier (Table 5). The two approaches showed relatively close agreement for the western glaciers, but diverged substantially in the eastern sector, where the thickness-derived volume loss was considerably greater than the estimates derived from DEM differencing. This discrepancy was driven largely by Stephenson Glacier, where the loss of relatively thick ice near the glacier terminus during lagoon expansion contributed most of the total volume loss (Fig. 5).

After standardization to the common 2000–2019 period, differences between the volume changes from ice thickness and DEM differencing ranged from −0.1 to + 0.1 km^3 for the western glaciers, and from −1.8 to + 0.0 km^3 for the eastern glaciers. Stephenson Glacier was the main contributor to the regional discrepancy between the two methods. Its thickness-derived volume change was -2.2 ± 0.7 km^3, compared with a DEM-differencing estimate of -0.4 ± 0.0 km^3, corresponding to a difference of -1.8 ± 0.7 km^3.

All glaciers excluding Stephenson collectively lost 1.6 ± 0.3 km^3 according to the ice thickness, while Stephenson Glacier alone lost 2.2 ± 0.5 km^3. For the remaining glaciers, the corresponding estimate derived from DEM differencing was -1.2 ± 0.0 km^3, giving a difference of 0.4 ± 0.3 km^3 between the two methods. Although this difference slightly exceeded the

https://doi.org/10.5194/egusphere-2026-7134
Preprint. Discussion started: 26 November 2026
© Author(s) 2026. CC BY 4.0 License.

combined 1σ uncertainty, it was not statistically significant at the 95% confidence level. At the individual-glacier scale, 20 of the remaining glaciers agreed within their combined 1σ uncertainties.

The significant discrepancy suggests that surface-elevation differencing does not capture a substantial component of the ice loss associated with terminus retreat into Stephenson Lagoon, particularly ice removed below the water surface. Although DEM differencing may include part of the volume loss associated with terminus retreat, it underestimates ice loss below the ocean or lake surface, particularly where grounded ice is replaced by water (Hock et al., 2026). Thus, incorporating subaqueous volume changes for rapidly retreating marine- or lake-terminating glaciers is important when total volume change is the quantity of interest (Kochtitzky et al., 2022; Zhang et al., 2023).

If we extend the relationship between glacier recession and proglacial lagoon development observed during 2000–2019 to the earlier 1947–2000 period, a similar pattern emerges. During this period, the combined volume loss of Compton, Brown, and Winston Glaciers accounted for 37 % of the total glacier volume loss across Heard Island. Compton and Brown Lagoons developed substantially during this period, after which their expansion largely ceased (Fig. S6). For Winston Lagoon, 52 % of its 2001 area had already been developed before 1947. From 1947 to 2019, Winston Lagoon continued to expand slowly and progressively.

Integrating the updated glacier area changes, mass-balance estimates, and glacier volume changes, we infer that the climatic drivers of glacier recession across Heard Island are likely similar. The episodic behaviour of some eastern glaciers, including Stephenson, Compton, Brown and Winston Glaciers, was clearly influenced by the development of proglacial lagoons. Frontal ablation through calving and subaqueous melt likely played an important role for lagoon-terminating glaciers (Sugiyama et al., 2021; Zhang et al., 2023). Future projections of glacier change on Heard Island should therefore account for the combined effects of climatic forcing, and proglacial lagoons, marine termini, and associated frontal and subaqueous processes.

5.3 Eco-evolutionary implications of glacier recession and landscape evolution

Glacier recession on Heard Island has substantially reorganized the island landscape, with ecological consequences extending beyond the loss of glacial ice. Given what is known of the terrestrial biota, and of responses of other organisms to glacial retreat, both in mountain glacier and polar settings (Lee et al., 2022; Winker et al. 2023; Gobbi et al., 2026), glacier recession on Heard Island is expected to have the following eco-evolutionary implications.

First, glacier recession exposes new ice-free substrate and provides new habitats for ecological colonization and ecosystem development (Lee et al., 2017, 2022). Between 1947 and 2019, the area of Heard Island not covered by glacier ice increased from approximately 78.6 to 142.3 km^2, corresponding to an increase from 21 % to 39 % of the reference island area of 368 km^2 (Geoscience Australia, 2026). The exposed ice-free land will enable significant upslope colonisation of landscapes by plants and animals, as will warming. Both responses have been recorded on other sub-Antarctic islands (Frenot et al. 1998; le Roux and McGeoch, 2008), though the responses are individualistic. Such change has been predicted by modelling (Davies et al., 2011). On Heard Island, the invasive grass Poa annua, a species known to take advantage of glacial recession (Frenot et al., 1998), is expanding its range (Scott and Kirkpatrick 2005), which may change landscapes that are otherwise mostly free of invasive alien species (Green and Woehler, 2006). Expansion of closed vegetation communities with glacial recession, increased liquid precipitation and increasing temperatures, will change the community composition of particular sites, given plant and animal habitat drivers, but what the balance will be between closed and open communities is difficult to predict.

Second, coalescence of areas previously isolated by glaciers, as has clearly happened in the east, and likely to proceed more generally (Fig. 5), is likely to lead to erosion of any population divergence established across the island. Elsewhere in polar and alpine regions, population separation through glaciation has driven speciation, while coalescence as a consequence of deglaciation has played a significant role in what is considered a form of extinction (Alcala and Vuilleumier, 2014; Winker et al., 2023). These processes are expected for Heard Island too. However, in some areas, glacier retreat has left proglacial lagoons

https://doi.org/10.5194/egusphere-2026-7134
Preprint. Discussion started: 26 November 2026
© Author(s) 2026. CC BY 4.0 License.

or coastal waters rather than exposed land, potentially limiting dispersal between terrestrial habitats (Fig. S6). It remains unclear to what extent these water barriers offset the gains in terrestrial habitat connectivity on Heard Island.

Third, temperature and precipitation are primary determinants of fitness for plant and invertebrate individuals and populations. Not only are broad scale conditions changing on the island (Fig. 9), but glacial influences on microclimates will also change with glacial recession. In the former case, at least some Heard Island species are known to be sensitive, on ecological and evolutionary timescales, to temperature and water availability (Chown and Klok 2003; Klok and Chown 2003, 2005; Chown et al. 2004), and significant responses are expected, though how these will play out is not yet clear (but see Davies et al. 2011). In the latter case, glacial landscapes often provide climate refuges for species (Gobbi et al., 2026) and these will be substantially altered, adding additional complexity.

Overall, significant eco-evolutionary responses are expected for the biota of Heard Island. The spatial and temporal reconstructions of glaciers presented here provide a framework against which contemporary phylogeographic and genomic patterns can be interpreted. Only substantial empirical and modelling work, building on studies such as this one and integrating ongoing continuous simulations of glacial change will, however, provide firm grounds for documenting and anticipating future eco-evolutionary change.

6 Conclusion

This study provides a spatially and temporally consistent reconstruction of glacier area, volume and mass change, and ice thickness, across Heard Island from 1947 to 2019. Glacier area decreased from 289.4 ± 5.6 km^2 in 1947 to 225.7 ± 2.5 km^2 in 2019, while glacier volume declined from 29.2 ± 6.1 to 19.8 ± 4.1 km^3. Glacier loss accelerated after 2000, with mean annual area and volume loss rates during 2000–2019 approximately 1.8 times those during 1947–2000. During 2000–2019, the mean glacier mass balance across Heard Island was −0.28 ± 0.02 m w.e. yr^{-1}, with substantially greater losses in the eastern sector (−0.53 ± 0.04 m w.e. yr^{-1}) than in the western sector (−0.21 ± 0.02 m w.e. yr^{-1}).

Stephenson Glacier showed the most negative mass balance (−1.10 ± 0.08 m w.e. yr^{-1}) and dominated the strong eastern-sector losses. If Stephenson Glacier is omitted, there are no strong west to east differences. The contrast was even more pronounced in the volume change estimates: the ice-thickness inversion indicated a volume loss of 2.2 ± 0.5 km^3 from 2000 to 2019, compared with only 0.4 ± 0.3 km^3 from DEM differencing. This discrepancy suggests that DEM differencing alone does not capture a substantial component of the loss associated with the removal of relatively thick ice near the glacier terminus during lagoon expansion.

Sensitivity experiments indicated that temporal mismatches between glacier outlines and DEMs can bias mass-balance estimates by 12–41 % and ice thickness estimates by 100–300 m, particularly for rapidly receding lagoon-terminating glaciers. These results highlight the importance of using temporally consistent glacier datasets when reconstructing long-term glacier change. They also provide a physical baseline for future work examining how continued deglaciation will reorganize land, water, habitat availability, and ecological connectivity across Heard Island.

Code availability

DEM co-registration was performed using xDEM v0.2.3 (xDEM contributors, 2026; https://pypi.org/project/xdem/0.2.3/). Glacier ice thickness was reconstructed using GlabTop2-py v2.1.1 (Terink, 2024; https://pypi.org/project/GlabTop2-py/2.1.1/). The Python scripts developed for data processing, analysis, and visualization in this study are available at GitHub (https://github.com/GlacierWeilin/Heard-Island-mass-balance-ice-thickness.git).

https://doi.org/10.5194/egusphere-2026-7134
Preprint. Discussion started: 26 November 2026
© Author(s) 2026. CC BY 4.0 License.

Data availability

The existing datasets used in this study are listed in Table 1 and are accessible through their respective sources. The newly derived glacier mass-balance estimates, and ice thickness datasets are available at GitHub (https://github.com/GlacierWeilin/Heard-Island-mass-balance-ice-thickness.git). The glacier and lagoon outlines are available upon request from WY or LGT.

Supplement link

The supplementary Table S1 and Figs. S1–S7 for this article are available at [].

Author contributions

Conceptualization, WY and ANM; methodology, WY and RH; glacier and lagoon mapping, LGT; formal analysis and visualization, WY; writing – original draft, WY; writing – original draft (text on Heard Island biology in Section 2 and 5.3), SLC; writing – review and editing, WY, LGT, RH, BJD, DDM, SLC, SST, JDS, and ANM; funding acquisition, ANM, RH, BJD, SLC, DDM, and JDS; supervision, ANM.

Competing interests

The authors declare no competing interests.

Acknowledgements

The Pléiades satellite data used in this study were provided by the Pléiades Glacier Observatory, funded by DINAMIS, the French national infrastructure for shared access to very high-resolution satellite imagery. We are very grateful to Etienne Berthier for his help in obtaining the Pléiades satellite product.

Financial support

This research was supported by the Australian Government through the Australian Research Council (ARC) Discovery Projects funding scheme (DP250100464) and the ARC Special Research Initiative (SRI) Securing Antarctica's Environmental Future (SR200100005). RH was supported by the European Research Council (ERC) under the European Union's Horizon Europe programme through the ERC-2022-ADG project GLACMASS (grant agreement No. 101096057).

Review statement

References

Alcala, N. and Vuilleumier, S.: Turnover and accumulation of genetic diversity across large time-scale cycles of isolation and connection of populations, Proc. R. Soc. B, 281, 20141369, https://doi.org/10.1098/rspb.2014.1369, 2014.

Allison, I. F. and Keage, P. L.: Recent changes in the glaciers of Heard Island, Polar Rec., 23, 255–272, https://doi.org/10.1017/S0032247400007099, 1986.

https://doi.org/10.5194/egusphere-2026-7134
Preprint. Discussion started: 26 November 2026
© Author(s) 2026. CC BY 4.0 License.

649 Baird, H. P., Shin, S., Oberprieler, R. G., Hullé, M., Vernon, P., Moon, K. L., Adams, R. H., McKenna, D. D., and Chown, S.
650 L.: Fifty million years of beetle evolution along the Antarctic Polar Front, Proc. Natl. Acad. Sci. USA, 118, e2017384118,
651 https://doi.org/10.1073/pnas.2017384118, 2021.
652 Balco, G.: A surprisingly large marine ice cap at Heard Island during the Last Glacial Maximum?, in: Antarctica: A Keystone
653 in a Changing World – Online Proceedings of the 10th ISAES, edited by: Cooper, A. K. and Raymond, C. R., U.S. Geological
654 Survey Open-File Report 2007-1047, Extended Abstract 147, 4 pp, https://pubs.usgs.gov/of/2007/1047/ea/of2007-
655 1047ea147.pdf, 2007.
656 Berthier, E., Le Bris, R., Mabileau, L., Testut, L., and Rémy, F.: Ice wastage on the Kerguelen Islands (49° S, 69° E) between
657 1963 and 2006, J. Geophys. Res.-Earth, 114, F03005, https://doi.org/10.1029/2008JF001192, 2009.
658 Berthier, E., Lebreton, J., Fontannaz, D., Hosford, S., Belart, J. M.-C., Brun, F., Andreassen, L. M., Menounos, B., and Blondel,
659 C.: The Pléiades Glacier Observatory: high-resolution digital elevation models and ortho-imagery to monitor glacier change,
660 The Cryosphere, 18, 5551–5571, https://doi.org/10.5194/tc-18-5551-2024, 2024.
661 Bosson, J. B., Huss, M., Cauvy-Fraunié, S., Clément, J. C., Costes, G., Fischer, M., Poulenard, J., and Arthaud, F.: Future
662 emergence of new ecosystems caused by glacial retreat, Nature, 620, 562–569, https://doi.org/10.1038/s41586-023-06302-2,
663 2023.
664 Budd, G. M.: Australian exploration of Heard Island, 1947–1971, Polar Rec., 43, 97–123,
665 https://doi.org/10.1017/S0032247407006080, 2007.
666 Carrivick, J. L., James, W. H. M., Grimes, M., Sutherland, J. L., and Lorrey, A. M.: Ice thickness and volume changes across
667 the Southern Alps, New Zealand, from the little ice age to present, Sci. Rep., 10, 13392, https://doi.org/10.1038/s41598-020-
668 70276-8, 2020.
669 Carrivick, J. L., Davies, M., Wilson, R., Davies, B. J., Gribbin, T., King, O., Rabatel, A., García, J.-L., and Ely, J. C.:
670 Accelerating glacier area loss across the Andes since the Little Ice Age, Geophys. Res. Lett., 51, e2024GL109154,
671 https://doi.org/10.1029/2024GL109154, 2024.
672 Cauvy-Fraunié, S. and Dangles, O.: A global synthesis of biodiversity responses to glacier retreat, Nat. Ecol. Evol., 3, 1675–
673 1685, https://doi.org/10.1038/s41559-019-1042-8, 2019.
674 Chown, S. L. and Klok, C. J.: Habitat use, diet and body size of Heard Island weevils, Polar Biol., 24, 706–712,
675 https://doi.org/10.1007/s003000100281, 2001.
676 Chown, S. L. and Klok, C. J.: Water-balance characteristics respond to changes in body size in subantarctic weevils, Physiol.
677 Biochem. Zool., 76, 634–643, https://doi.org/10.1086/376919, 2003.
678 Chown, S. L., Klok, C. J., and McGeoch, M. A.: Weather to go out: activity of Bothrometopus brevis (Curculionidae) at Heard
679 Island, Polar Biol., 27, 217–221, https://doi.org/10.1007/s00300-003-0579-8, 2004.
680 Chown, S. L., Bergstrom, D. M., Houghton, M., Kiefer, K., Terauds, A., and Leihy, R. I.: Invasive species impacts on sub-
681 Antarctic Collembola support the Antarctic climate-diversity-invasion hypothesis, Soil Biol. Biochem., 166, 108579,
682 https://doi.org/10.1016/j.soilbio.2022.108579, 2022.
683 Cook, A. J., Poncet, S., Cooper, A. P. R., Herbert, D. J., and Christie, D.: Glacier retreat on South Georgia and implications
684 for the spread of rats, Antarct. Sci., 22, 255–263, https://doi.org/10.1017/S0954102010000064, 2010.
685 Davies, B. J., Atkinson, A., Banwell, A. F., Brandon, M., Caton Harrison, T., Convey, P., De Rydt, J., Dodds, K., Downie, R.,
686 Edwards, T. L., Gilbert, E., Hubbard, B., Hughes, K. A., Marshall, G. J., Orr, A., Rogelj, J., Seroussi, H., Siegert, M., Stroeve,
687 J., and Rumble, J.: The Antarctic Peninsula under present day climate and future low, medium-high and very high emissions
688 scenarios, Front. Environ. Sci., 13, 1730203, https://doi.org/10.3389/fenvs.2025.1730203, 2026.
689 Davies, K. F., Melbourne, B. A., McClenahan, J. L., and Tuff, T.: Statistical models for monitoring and predicting effects of
690 climate change and invasion on the free-living insects and a spider from sub-Antarctic Heard Island, Polar Biol., 34, 119–125,
691 https://doi.org/10.1007/s00300-010-0865-1, 2011.

https://doi.org/10.5194/egusphere-2026-7134
Preprint. Discussion started: 26 November 2026
© Author(s) 2026. CC BY 4.0 License.

Donoghue, S. L.: Changes in the morphology, mass balance and dynamics of Brown Glacier, Heard Island, with comparison to the surrounding sub-Antarctic islands, PhD thesis, University of Tasmania, Hobart, Australia, https://doi.org/10.25959/23233313, 2009.

Dussaillant, I., Berthier, E., Brun, F., Masiokas, M., Hugonnet, R., Favier, V., Rabatel, A., Pitte, P., and Ruiz, L.: Two decades of glacier mass loss along the Andes, Nat. Geosci., 12, 802–808, https://doi.org/10.1038/s41561-019-0432-5, 2019.

Dussaillant, I., Hugonnet, R., Huss, M., Berthier, E., Bannwart, J., Paul, F., and Zemp, M.: Annual mass change of the world's glaciers from 1976 to 2024 by temporal downscaling of satellite data with in situ observations, Earth Syst. Sci. Data, 17, 1977–2006, https://doi.org/10.5194/essd-17-1977-2025, 2025.

EROS Center: Landsat 7 Enhanced Thematic Mapper Plus Level-2, Collection 2, U.S. Geological Survey [data set], https://doi.org/10.5066/P9C7I13B (last access: 12 October 2026), 2020.

European Space Agency: Copernicus DEM – Global and European Digital Elevation Model (COP-DEM), GLO-30, European Space Agency [data set], https://doi.org/10.5270/ESA-c5d3d65 (last access: 12 October 2026), 2021.

Farías-Barahona, D., Sommer, C., Sauter, T., Bannister, D., Seehaus, T. C., Malz, P., Casassa, G., Mayewski, P. A., Turton, J. V., and Braun, M. H.: Detailed quantification of glacier elevation and mass changes in South Georgia, Environ. Res. Lett., 15, 034036, https://doi.org/10.1088/1748-9326/ab6b32, 2020.

Farinotti, D., Huss, M., Fürst, J. J., Landmann, J., Machguth, H., Maussion, F., and Pandit, A.: A consensus estimate for the ice thickness distribution of all glaciers on Earth, Nat. Geosci., 12, 168–173, https://doi.org/10.1038/s41561-019-0300-3, 2019.

Favier, V., Verfaillie, D., Berthier, E., Menegoz, M., Jomelli, V., Kay, J. E., Ducret, L., Malbéteau, Y., Brunstein, D., Gallée, H., Park, Y.-H., and Rinterknecht, V.: Atmospheric drying as the main driver of dramatic glacier wastage in the southern Indian Ocean, Sci. Rep., 6, 32396, https://doi.org/10.1038/srep32396, 2016.

Fox-Kemper, B., Hewitt, H. T., Xiao, C., Aðalgeirsdóttir, G., Drijfhout, S. S., Edwards, T. L., Golledge, N. R., Hemer, M., Kopp, R. E., Krinner, G., Mix, A., Notz, D., Nowicki, S., Nurhati, I. S., Ruiz, L., Sallée, J.-B., Slangen, A. B. A., and Yu, Y.: Ocean, Cryosphere and Sea Level Change, in: Climate Change 2021: The Physical Science Basis. Contribution of Working Group I to the Sixth Assessment Report of the Intergovernmental Panel on Climate Change, edited by: Masson-Delmotte, V., Zhai, P., Pirani, A., Connors, S. L., Péan, C., Berger, S., Caud, N., Chen, Y., Goldfarb, L., Gomis, M. I., Huang, M., Leitzell, K., Lonnoy, E., Matthews, J. B. R., Maycock, T. K., Waterfield, T., Yelekçi, O., Yu, R., and Zhou, B., Cambridge University Press, Cambridge, UK and New York, NY, USA, 1211–1362, https://doi.org/10.1017/9781009157896.011, 2021.

Frank, T., van Pelt, W. J. J., Rounce, D. R., Jouvet, G., and Hock, R.: Global glacier-free topography reveals a large potential for future lakes in presently ice-covered terrain, Nat. Commun., 17, 3985, https://doi.org/10.1038/s41467-026-72548-9, 2026.

Frenot, Y., Gloaguen, J.C., Cannavacciuolo, M., and Bellido, A.: Primary succession on glacier forelands in the subantarctic Kerguelen Islands, J. Veg. Sci., 9, 75–84, https://doi.org/10.2307/3237225, 1998.

Frey, H., Machguth, H., Huss, M., Huggel, C., Bajracharya, S., Bolch, T., Kulkarni, A., Linsbauer, A., Salzmann, N., and Stoffel, M.: Estimating the volume of glaciers in the Himalayan–Karakoram region using different methods, The Cryosphere, 8, 2313–2333, https://doi.org/10.5194/tc-8-2313-2014, 2014.

Gardelle, J., Berthier, E., and Arnaud, Y.: Impact of resolution and radar penetration on glacier elevation changes computed from DEM differencing, J. Glaciol., 58, 419–422, https://doi.org/10.3189/2012JoG11J175, 2012.

Geoscience Australia: Heard and McDonald Islands, Australian Government, https://www.ga.gov.au/scientific-topics/national-location-information/geography/external-territories (last access: 13 November 2026), 2026.

Gobbi, M., Valle, B., Brambilla, M., Tampucci, D., and Caccianiga, M.: Global threats, local opportunities: ice-related landforms provide refugia for high-elevation plants and arthropods, Ecography, 2026, e08695, https://doi.org/10.1002/ecog.08695, 2026.

Green, K. and Woehler, E. (Eds.): Heard Island: Southern Ocean Sentinel, Surrey Beatty & Sons, Chipping Norton, NSW, Australia, 270 pp., ISBN 0949324981, 2006.

https://doi.org/10.5194/egusphere-2026-7134
Preprint. Discussion started: 26 November 2026
© Author(s) 2026. CC BY 4.0 License.

Haeberli, W. and Hoelzle, M.: Application of inventory data for estimating characteristics of and regional climate-change effects on mountain glaciers: a pilot study with the European Alps, Ann. Glaciol., 21, 206–212, https://doi.org/10.3189/S0260305500015834, 1995.

Hall, K.: Quaternary glaciation of the sub-Antarctic Islands, in: Quaternary Glaciations – Extent and Chronology, Volume 2, Part C, edited by: Ehlers, J. and Gibbard, P. L., Elsevier, Amsterdam, the Netherlands, 339–345, https://doi.org/10.1016/S1571-0866(04)80140-4, 2004.

Harris, U.: Heard and McDonald Islands – Bathymetric data created for the 1:1,000,000 bathymetric map, Version 1, Australian Antarctic Data Centre [data set], https://data.aad.gov.au/metadata/heard_bathy_gis (last access: 15 October 2026), 2004.

Hersbach, H., Bell, B., Berrisford, P., Hirahara, S., Horányi, A., Muñoz-Sabater, J., Nicolas, J., Peubey, C., Radu, R., Schepers, D., Simmons, A., Soci, C., Abdalla, S., Abellan, X., Balsamo, G., Bechtold, P., Biavati, G., Bidlot, J., Bonavita, M., De Chiara, G., Dahlgren, P., Dee, D., Diamantakis, M., Dragani, R., Flemming, J., Forbes, R., Fuentes, M., Geer, A., Haimberger, L., Healy, S., Hogan, R. J., Hólm, E., Janisková, M., Keeley, S., Laloyaux, P., Lopez, P., Lupu, C., Radnoti, G., de Rosnay, P., Rozum, I., Vamborg, F., Villaume, S., and Thépaut, J.-N.: The ERA5 global reanalysis, Q. J. Roy. Meteor. Soc., 146, 1999–2049, https://doi.org/10.1002/qj.3803, 2020.

Hock, R., Rasul, G., Adler, C., Cáceres, B., Gruber, S., Hirabayashi, Y., Jackson, M., Kääb, A., Kang, S., Kutuzov, S., Milner, Al., Molau, U., Morin, S., Orlove, B., and Steltzer, H.: High Mountain Areas, in: IPCC Special Report on the Ocean and Cryosphere in a Changing Climate, edited by: Pörtner, H.-O., Roberts, D. C., Masson-Delmotte, V., Zhai, P., Tignor, M., Poloczanska, E., Mintenbeck, K., Alegría, A., Nicolai, M., Okem, A., Petzold, J., Rama, B., and Weyer, N. M., Cambridge University Press, Cambridge, UK and New York, NY, USA, 131–202, https://doi.org/10.1017/9781009157964.004, 2019.

Hock, R., Huss, M., Berthier, E., Braun, M., Gardner, A. S., Wouters, B., and Zemp, M.: Toward improved comparability of glacier mass-balance estimates: challenges and recommendations, J. Glaciol., 72, e49, https://doi.org/10.1017/jog.2026.10158, 2026.

Hugonnet, R., McNabb, R., Berthier, E., Menounos, B., Nuth, C., Girod, L., Farinotti, D., Huss, M., Dussaillant, I., Brun, F., and Kääb, A.: Accelerated global glacier mass loss in the early twenty-first century, Nature, 592, 726–731, https://doi.org/10.1038/s41586-021-03436-z, 2021.

Hugonnet, R., Brun, F., Berthier, E., Dehecq, A., Mannerfelt, E. S., Eckert, N., and Farinotti, D.: Uncertainty analysis of digital elevation models by spatial inference from stable terrain, IEEE J. Sel. Top. Appl. Earth Obs. Remote Sens., 15, 6456–6472, https://doi.org/10.1109/JSTARS.2022.3188922, 2022.

Huss, M.: Density assumptions for converting geodetic glacier volume change to mass change, The Cryosphere, 7, 877–887, https://doi.org/10.5194/tc-7-877-2013, 2013.

Hutter, K.: Theoretical Glaciology: Material Science of Ice and the Mechanics of Glaciers and Ice Sheets, D. Reidel Publishing Company, Dordrecht, the Netherlands, 510 pp., https://doi.org/10.1007/978-94-015-1167-4, 1983.

Kiernan, K. and McConnell, A.: Glacier retreat and melt-lake expansion at Stephenson Glacier, Heard Island World Heritage Area, Polar Rec., 38(207), 297–308, https://doi.org/10.1017/S0032247400017988, 2002.

Klok, C. J. and Chown, S. L.: Resistance to temperature extremes in sub-Antarctic weevils: interspecific variation, population differentiation and acclimation, Biol. J. Linn. Soc., 78, 401–414, https://doi.org/10.1046/j.1095-8312.2003.00154.x, 2003.

Klok, C. J. and Chown, S. L.: Inertia in physiological traits: Embryonopsis halticella caterpillars (Yponomeutidae) across the Antarctic Polar Frontal Zone, J. Insect Physiol., 51, 87–97, https://doi.org/10.1016/j.jinsphys.2004.11.011, 2005.

Kochtitzky, W., Copland, L., Van Wychen, W., Hugonnet, R., Hock, R., Dowdeswell, J. A., Benham, T., Strozzi, T., Glazovsky, A., Lavrentiev, I., Rounce, D. R., Millan, R., Cook, A., Dalton, A., Jiskoot, H., Cooley, J., Jania, J., and Navarro, F.: The unquantified mass loss of Northern Hemisphere marine-terminating glaciers from 2000–2020, Nat. Commun., 13, 5835, https://doi.org/10.1038/s41467-022-33231-x, 2022.

https://doi.org/10.5194/egusphere-2026-7134
Preprint. Discussion started: 26 November 2026
© Author(s) 2026. CC BY 4.0 License.

Lee, J. R., Raymond, B., Bracegirdle, T. J., Chadès, I., Fuller, R. A., Shaw, J. D., and Terauds, A.: Climate change drives expansion of Antarctic ice-free habitat, Nature, 547, 49–54, https://doi.org/10.1038/nature22996, 2017.

Lee, J. R., Waterman, M. J., Shaw, J. D., Bergstrom, D. M., Lynch, H. J., Wall, D. H., and Robinson, S. A.: Islands in the ice: potential impacts of habitat transformation on Antarctic biodiversity, Glob. Change Biol., 28, 5865–5880, https://doi.org/10.1111/gcb.16331, 2022.

le Roux, P. C. and McGeoch, M. A.: Rapid range expansion and community reorganization in response to warming, Glob. Change Biol., 14, 2950–2962, https://doi.org/10.1111/j.1365-2486.2008.01687.x, 2008.

Maffezzoli, N., Rignot, E., Barbante, C., Morlighem, M., Petersen, T. C., and Vascon, S.: Machine-learned global glacier ice volumes, Sci. Data, 13, 1104, https://doi.org/10.1038/s41597-026-07744-9, 2026.

Menne, M. J., Durre, I., Korzeniewski, B., McNeill, S., Thomas, K., Yin, X., Anthony, S., Ray, R., Vose, R. S., Gleason, B. E., and Houston, T. G.: Global Historical Climatology Network – Daily (GHCN-Daily), Version 3, NOAA National Climatic Data Center [data set], https://doi.org/10.7289/V5D21VHZ (last access: 12 October 2026), 2012.

Millan, R., Mouginot, J., Rabatel, A., and Morlighem, M.: Ice velocity and thickness of the world's glaciers, Nat. Geosci., 15, 124–129, https://doi.org/10.1038/s41561-021-00885-z, 2022.

Minowa, M., Schaefer, M., Sugiyama, S., Sakakibara, D., and Skvarca, P.: Frontal ablation and mass loss of the Patagonian icefields, Earth Planet. Sci. Lett., 561, 116811, https://doi.org/10.1016/j.epsl.2021.116811, 2021.

Morland, L. W.: Thermomechanical balances of ice sheet flows, Geophys. Astrophys. Fluid Dyn., 29, 237–266, https://doi.org/10.1080/03091928408248191, 1984.

Muñoz-Sabater, J., Dutra, E., Agustí-Panareda, A., Albergel, C., Arduini, G., Balsamo, G., Boussetta, S., Choulga, M., Harrigan, S., Hersbach, H., Martens, B., Miralles, D. G., Piles, M., Rodríguez-Fernández, N. J., Zsoter, E., Buontempo, C., and Thépaut, J.-N.: ERA5-Land: a state-of-the-art global reanalysis dataset for land applications, Earth Syst. Sci. Data, 13, 4349–4383, https://doi.org/10.5194/essd-13-4349-2021, 2021.

NASA JPL: NASADEM SRTM-only Height and Height Precision Mosaic Global 1 arc second V001, NASA Land Processes Distributed Active Archive Center [data set], https://doi.org/10.5067/MEASURES/NASADEM/NASADEM_SHHP.001 (last access: 14 August 2026), 2020.

NASA/METI/AIST/Japan Spacesystems and U.S./Japan ASTER Science Team: ASTER Global Digital Elevation Model V003, NASA Land Processes Distributed Active Archive Center [data set], https://doi.org/10.5067/ASTER/ASTGTM.003 (last access: 14 August 2026), 2019.

Nuth, C. and Kääb, A.: Co-registration and bias corrections of satellite elevation data sets for quantifying glacier thickness change, The Cryosphere, 5, 271–290, https://doi.org/10.5194/tc-5-271-2011, 2011.

RGI Consortium: Randolph Glacier Inventory – A Dataset of Global Glacier Outlines, Version 6.0, NASA National Snow and Ice Data Center Distributed Active Archive Center [data set], https://doi.org/10.7265/4m1f-gd79 (last access: 12 October 2026), 2017.

RGI Consortium: Randolph Glacier Inventory – A Dataset of Global Glacier Outlines, Version 7.0, NASA National Snow and Ice Data Center Distributed Active Archive Center [data set], https://doi.org/10.5067/F6JMOVY5NAVZ (last access: 12 October 2026), 2023.

Scott, J. J. and Kirkpatrick, J. B.: Changes in subantarctic Heard Island vegetation at sites occupied by Poa annua, 1987–2000, Arct. Antarct. Alp. Res., 37, 366–371, https://doi.org/10.1657/1523-0430%282005%29037%5B0366%3ACISHIV%5D2.0.CO%3B2, 2005.

Sugiyama, S., Minowa, M., Fukamachi, Y., Hata, S., Yamamoto, Y., Sauter, T., Schneider, C., and Schaefer, M.: Subglacial discharge controls seasonal variations in the thermal structure of a glacial lake in Patagonia, Nat. Commun., 12, 6301, https://doi.org/10.1038/s41467-021-26578-0, 2021.

https://doi.org/10.5194/egusphere-2026-7134
Preprint. Discussion started: 26 November 2026
© Author(s) 2026. CC BY 4.0 License.



Terink, W.: GlabTop2-py (version 2.1.1), PyPI [code], https://pypi.org/project/GlabTop2-py/2.1.1/ (last access: 12 October 2026), 2024.

The GlaMBIE Team: Community estimate of global glacier mass changes from 2000 to 2023, Nature, 639, 382–388, https://doi.org/10.1038/s41586-024-08545-z, 2025.

The WGMS Network: Global glacier mass change in 2025, Nat. Rev. Earth Environ., 7, 213–215, https://doi.org/10.1038/s43017-026-00777-z, 2026.

Thost, D. E. and Truffer, M.: Glacier recession on Heard Island, Southern Indian Ocean, Arct. Antarct. Alp. Res., 40, 199–214, https://doi.org/10.1657/1523-0430(06-084)[THOST]2.0.CO;2, 2008.

Tielidze, L. G., Mackintosh, A. N., and Yang, W.: Glacier inventories reveal an acceleration of Heard Island glacier loss over recent decades, The Cryosphere, 19, 2677–2694, https://doi.org/10.5194/tc-19-2677-2025, 2025.

UNESCO World Heritage Centre: Heard and McDonald Islands, World Heritage List, property no. 577, https://whc.unesco.org/en/list/577/ (last access: 12 October 2026), 1997.

WGMS: Annual mass-change estimates for the world's glaciers (version 2026-02-10), World Glacier Monitoring Service, Zurich, Switzerland [data set], https://doi.org/10.5904/wgms-amce-2026-02-10 (last access: 12 October 2026), 2026.

Winker, K., Withrow, J. J., Gibson, D. D., and Pruett, C. L.: Beringia as a high-latitude engine of avian speciation, Biol. Rev., 98, 1081–1099, https://doi.org/10.1111/brv.12945, 2023.

xDEM contributors: xDEM (version 0.2.3), PyPI [code], https://pypi.org/project/xdem/0.2.3/, 2026.

Yang, R., Hock, R., Kang, S., Shangguan, D., and Guo, W.: Glacier mass and area changes on the Kenai Peninsula, Alaska, 1986–2016, J. Glaciol., 66(258), 603–617, https://doi.org/10.1017/jog.2020.32, 2020.

Zekollari, H., Huss, M., Farinotti, D., and Lhermitte, S.: Ice-dynamical glacier evolution modeling – A review, Rev. Geophys., 60, e2021RG000754, https://doi.org/10.1029/2021RG000754, 2022.

Zemp, M., Huss, M., Thibert, E., Eckert, N., McNabb, R., Huber, J., Barandun, M., Machguth, H., Nussbaumer, S. U., Gärtner-Roer, I., Thomson, L., Paul, F., Maussion, F., Kutuzov, S., and Cogley, J. G.: Global glacier mass changes and their contributions to sea-level rise from 1961 to 2016, Nature, 568, 382–386, https://doi.org/10.1038/s41586-019-1071-0, 2019.

Zhang, G., Bolch, T., Yao, T., Rounce, D. R., Chen, W., Veh, G., King, O., Allen, S. K., Wang, M., and Wang, W.: Underestimated mass loss from lake-terminating glaciers in the greater Himalaya, Nat. Geosci., 16, 333–338, https://doi.org/10.1038/s41561-023-01150-1, 2023.